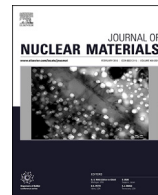




Contents lists available at ScienceDirect

Journal of Nuclear Materials

journal homepage: www.elsevier.com/locate/jnucmat

A review of microstructural features in fast reactor mixed oxide fuels

Riley Parrish, Assel Aitkaliyeva*

University of Florida, Department of Materials Science and Engineering, Gainesville, FL, 32611, United States

ARTICLE INFO

Article history:

Received 16 March 2018

Received in revised form

7 May 2018

Accepted 29 May 2018

Available online xxx

Keywords:

Mixed oxide fuel

Microstructure

Restructuring

Fission products

Agglomeration

Fuel-cladding chemical interaction

Experimental techniques

ABSTRACT

As an alternative to traditional uranium dioxide (UO_2) fuels, mixed oxide (MOX) fuels were developed to dispose of industrial and military stores of plutonium (Pu) through the incorporation of plutonium dioxide (PuO_2) powder into a UO_2 base fuel. The high temperature and chemical stability characteristic of oxide fuels would be maintained, while the added Pu would ultimately be eliminated from long term storage. Plutonium could be extracted from spent light water reactor (LWR) fuels, acting as an additional step to close the fuel cycle and mitigate potential environmental or proliferation concerns. This review summarizes the primary features associated with fast reactor MOX fuels, including fuel restructuring, actinide redistribution, solid fission products, plutonium agglomerates, joint oxide gain, and fuel-cladding chemical interaction. A summary of research efforts within the last 10 years and directions for future research are discussed.

© 2018 Elsevier B.V. All rights reserved.

Contents

| | |
|---|----|
| 1. Introduction | 00 |
| 2. Restructuring | 00 |
| 3. Central void formation and Pu redistribution | 00 |
| 4. Pu agglomerates | 00 |
| 5. Solid fission products | 00 |
| 5.1. Metallic inclusions | 00 |
| 5.2. Oxide phases | 00 |
| 5.3. Impact on fuel performance | 00 |
| 6. Joint-Oxide Gain | 00 |
| 7. FCCI | 00 |
| 8. Recent research trends | 00 |
| 9. Summary of research outcomes to date | 00 |
| 10. Areas of improvement | 00 |
| 11. Recommendations | 00 |
| References | 00 |

1. Introduction

The push for Generation IV Sodium-cooled Fast Reactor (SFR) technology has breathed new life into the prospects of MOX as a next generation fuel source [1]. Microstructural changes, fuel-cladding chemical interaction (FCCI) formation, and thermal property evolution are only a few of the challenges that need to be

* Corresponding author. 156 Rhines Hall, Department of Materials Science and Engineering, University of Florida, PO Box 116400, Gainesville, FL, 32611-6400, United States.

E-mail addresses: rileyparrish@ufl.edu (R. Parrish), aitkaliyeva@mse.ufl.edu (A. Aitkaliyeva).

addressed [2] in order to safely implement advanced MOX fuels in Generation IV reactors and beyond.

MOX fuels offer a considerable number of challenges from a materials science perspective. Fast breeder reactors (FBR's) fueled with MOX run at higher temperatures than LWR fuels [3], leading to differing fuel properties depending on burnup, height in fuel pin, or radial position in a given pellet. Fission product phases and evolving microstructures create highly localized properties that can differ significantly from the bulk fuel. Stoichiometry and Pu content are important factors that dictate thermal properties [4], ultimately influencing fuel safety and efficiency. In order to properly predict and model the effects of microstructure on fuel properties, it is important to understand the chemical nature and structure of these products over the lifetime of the fuel. This review will discuss phenomena unique to or primarily concerning fast reactor MOX fuel research. Due to the vast knowledge pool that already exists with standard UO₂, the scope of this review will not conduct an extensive review of all oxide fuels. Analysis of the microstructural features of MOX fuels and their implications on macroscale properties will be the primary thrust of this paper.

2. Restructuring

Oxide nuclear fuels are commonly touted for their outstanding high temperature capabilities under irradiation, outperforming their metallic fuel counterparts with higher melting temperatures, and having lower coefficients of thermal expansion than carbides and nitrides. However, with this stability comes the tradeoff of low thermal conductivity. Due to the inherent low thermal transport capabilities of the ceramic fuels, a temperature gradient is formed along the radius of the fuel pellet, with the hottest region at the center of the pellet and coolest near the cladding. The inability of the fuel to quickly and efficiently manage heat acts as an annealing process, leading to a grain growth and restructuring process. Restructuring makes long term irradiation performance predictions exceedingly complex due to the highly localized nature of the fuel properties. Fig. 1 shows an example of a low burnup, restructured MOX fuel pellet. It is not sufficient to predict the behavior of an entire fuel assembly using a singular microstructural approximation, as each region has a unique contribution to the macroscale fuel performance. While many of the features discussed have been commonly observed in UO₂ fuels for decades, PuO₂ additions further complicate the predictability of MOX fuels. For this reason, it is worth exploring the overall nature of MOX fuel evolution as it pertains to key operating parameters.

As described by Lambert and Strain [6], Pu bearing fast reactor oxide fuels display four defining regions of a restructured pellet: the central void, the columnar grain growth region, the equiaxed grain growth region, and the as-sintered region (Fig. 2). The center of the fuel rod experiences the highest peak temperatures and highest linear heating rates, forming coarse, elongated grains that grow radially toward the outer rim of the fuel. The equiaxed region consists of grains that have undergone significant growth when compared to the un-irradiated samples, while the outermost region of the pellet largely resembles the microstructure of the sintered pellet before irradiation. Variations in the overall structure of the pellet will exist as a result of the operating parameters, such as fuel pin linear heating rate (LHR), burnup, or centerline temperature of the fuel. Empirical data on the minimum temperature needed to initiate grain growth in each characteristic region during irradiation is unavailable due to the difficult nature of the measurements. Sari [7] has developed models for grain growth in two separate stoichiometries of fast reactor MOX fuels based on temperature and initial grain size, but does not take into account the effects of radiation assisted diffusion and fission product presence.

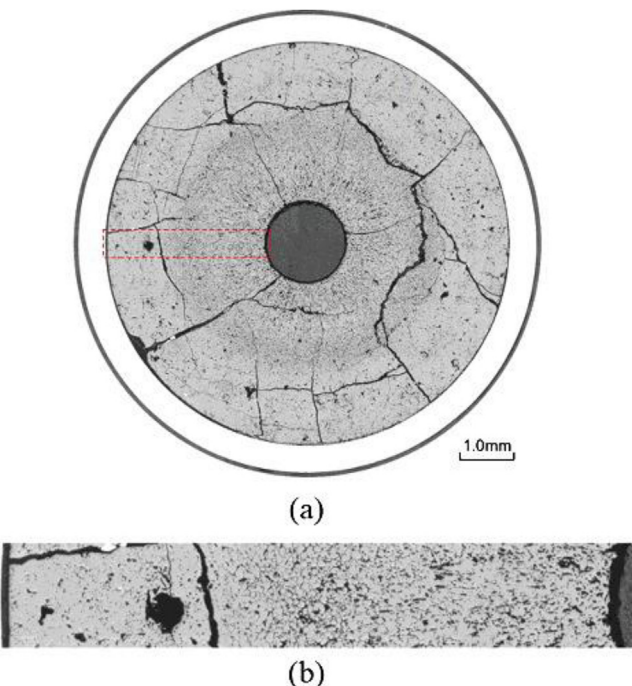


Fig. 1. a.) Microstructure of restructured hollow MOX fuel pellet irradiated to 30,310 MWd/t at a linear heating rate of 443 W cm^{-1} and b.) an enlarge image of the cutout section highlighted in red [5]. (For interpretation of the references to colour in this figure legend, the reader is referred to the Web version of this article.)

Approximations of the boundary temperatures may be modelled or estimated, but there remains uncertainty in the accuracy of such estimates. As a result, it is difficult to define or measure distinct threshold temperatures for restructuring in fast reactor MOX fuels.

3. Central void formation and Pu redistribution

Central voids have been shown to appear in irradiation times as short as 10 min [9], demonstrating that the appearance and size of the central void is formed as a result of fuel temperature and linear heating rate rather than explicitly on fuel burnup state [10–13]. Fig. 3 demonstrates the effects of linear heating rates and irradiation time on the restructuring and central void formation processes. The central void forms from the accumulation of voids and pores present in the fuel along a thermal gradient. Specifically within the columnar grain region of an irradiated fuel pellet, the pores migrate up the temperature gradient toward the center at varying rates depending on their starting size [10,14]. Fig. 4 shows a representation of the types of pores that form during reactor operation in oxide fuels. The smallest spherical pores are highly mobile, being able to quickly and easily move through the restructured region. Intermediate sized pores become flat and elongated as they travel towards the fuel centers, leaving streaks at the tips of the voids as they travel. These "lenticular" voids are the most readily identifiable porosity feature in the irradiated MOX fuels due to their distinct shape. The largest voids, usually starting as fabricated porosity in the fresh fuel, are the least stable of the three regimes, creating the appearances of long streaks radially pointing toward the fuel center.

The formation of a central void and the movement of pores leads to a redistribution of plutonium occurring during the early stages of irradiation [13,16–29]. Similar to central void formation, the redistribution can occur on times scales as short as 10 min. This redistribution manifests itself in a spike in Pu concentration

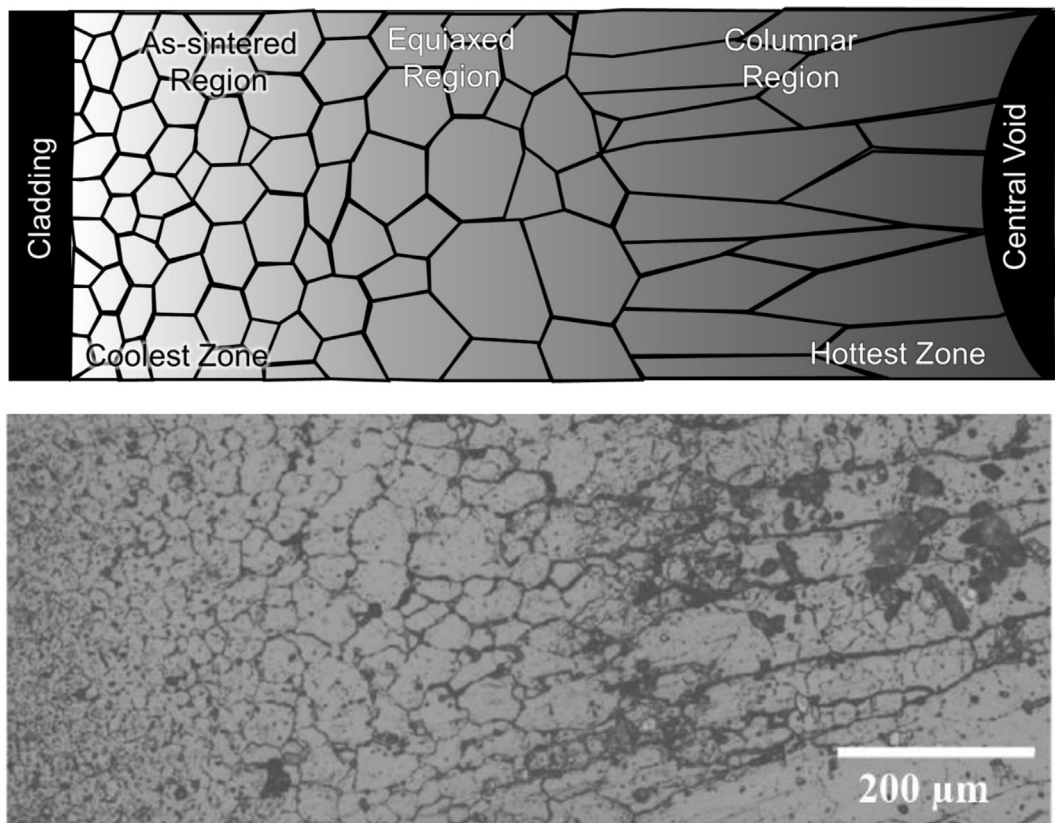


Fig. 2. a.) Schematic of oxide fuel restructuring, demonstrating the characteristic structures of the columnar, equiaxed, and as-sintered regions of the fuel. The darkest part of the gradient indicates the hottest part of the fuel, while the lightest section indicates the coolest, and b.) microstructural comparison of irradiated 29.1 wt% PuO_2 MOX fuel at 112 GWD t^{-1} demonstrating the corresponding regions seen in the schematic drawing [8].

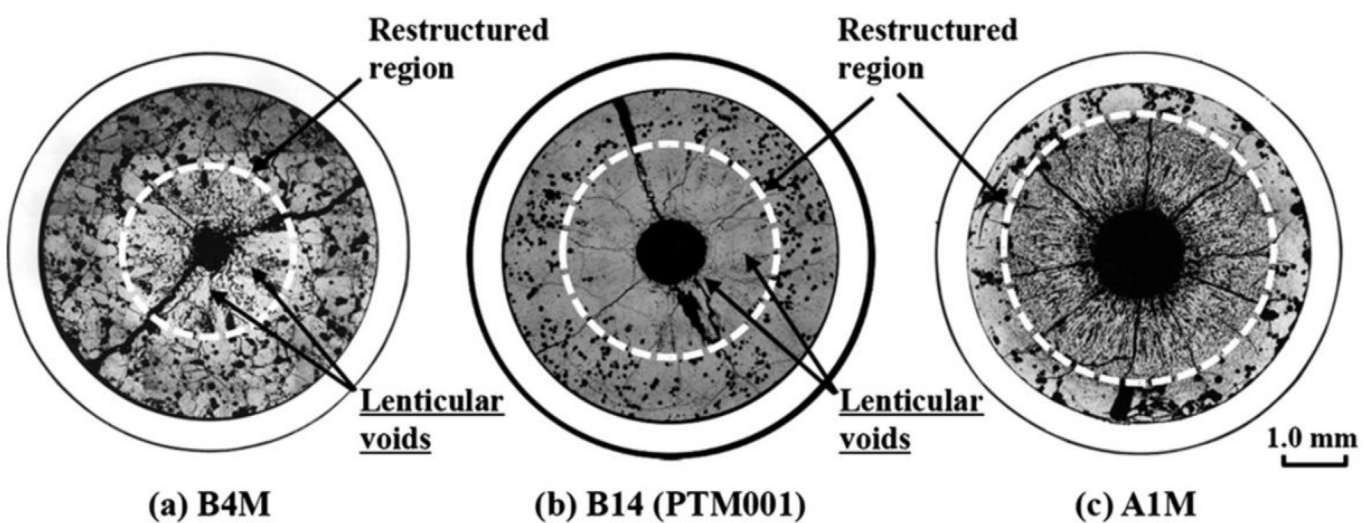


Fig. 3. Microstructural comparison of Am doped MOX irradiated for a.) 3 h, 377 W cm^{-2} linear heating rate (LHR), b.) 48 h at 386 W cm^{-2} , followed by 10 min at 470 W cm^{-2} , and c.) 480 W cm^{-2} until a burnup of 42 MW d kg^{-1} was reached [13].

surrounding the central void, anywhere between 10% and 70% increase in as-fabricated concentration. Similar behavior has been demonstrated with other minor actinides, such as americium [13,27–29], in which the redistribution gradient is much steeper near the central void. Fig. 5 demonstrates the redistribution phenomenon of actinides, showing a distinct increase in Pu and Am near the central void accompanied by a depletion of U in the

associated region. This redistribution becomes inherently problematic when trying model fuel behavior and design reactor systems, as the high actinide concentrations near the centerline has been shown to increase centerline temperatures upwards of 100°C and lower the melting temperature of the pellet center [18,24,25].

The prevailing explanation for this phenomenon is an evaporation-condensation process in which the fuel at the edge of

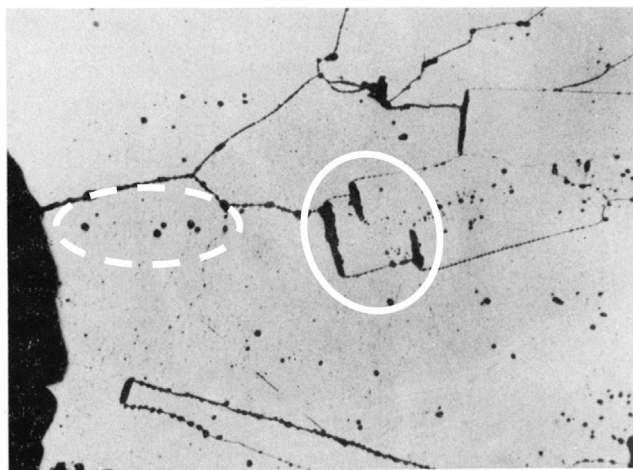


Fig. 4. Photomicrograph of oxide fuel showing the representative shape of lenticular (solid line) and small, round (dashed line) that migrate toward the central void (seen in far left of image) [15].

the pore closest to the centerline becomes gaseous inside the pore and deposit itself on the cooler region of the pore closest to the cladding [17,18,20–22,25,30,31]. UO_2 is the more volatile of the U-Pu heavy metal species present in the fuel matrix, with the high oxygen potential leading to a high partial pressure of UO_3 within the self-contained pores. In the absence of U, enriched regions of PuO_2 are left behind and deposited at the leading edge of the central void as the porosity agglomerates in the fuel center.

The evaporation-condensation theory was predominantly accepted by the experimental community, but critics claimed that the understanding of thermodynamics and kinetics at the time could not corroborate the pore velocities necessary to show central void formation and Pu redistribution on the observed time scales [32–35]. However, no experimentally proven substitution has been put forth as a replacement theory to the observed features. One such theory gave increased importance to transport pathways such as fuel cracks formed during thermal cycling or fission gas bubbles accumulating at the grain boundaries [32,33]. This theory never gained much traction among the experimentalists and was additionally disputed by the computational community [36]. The crack

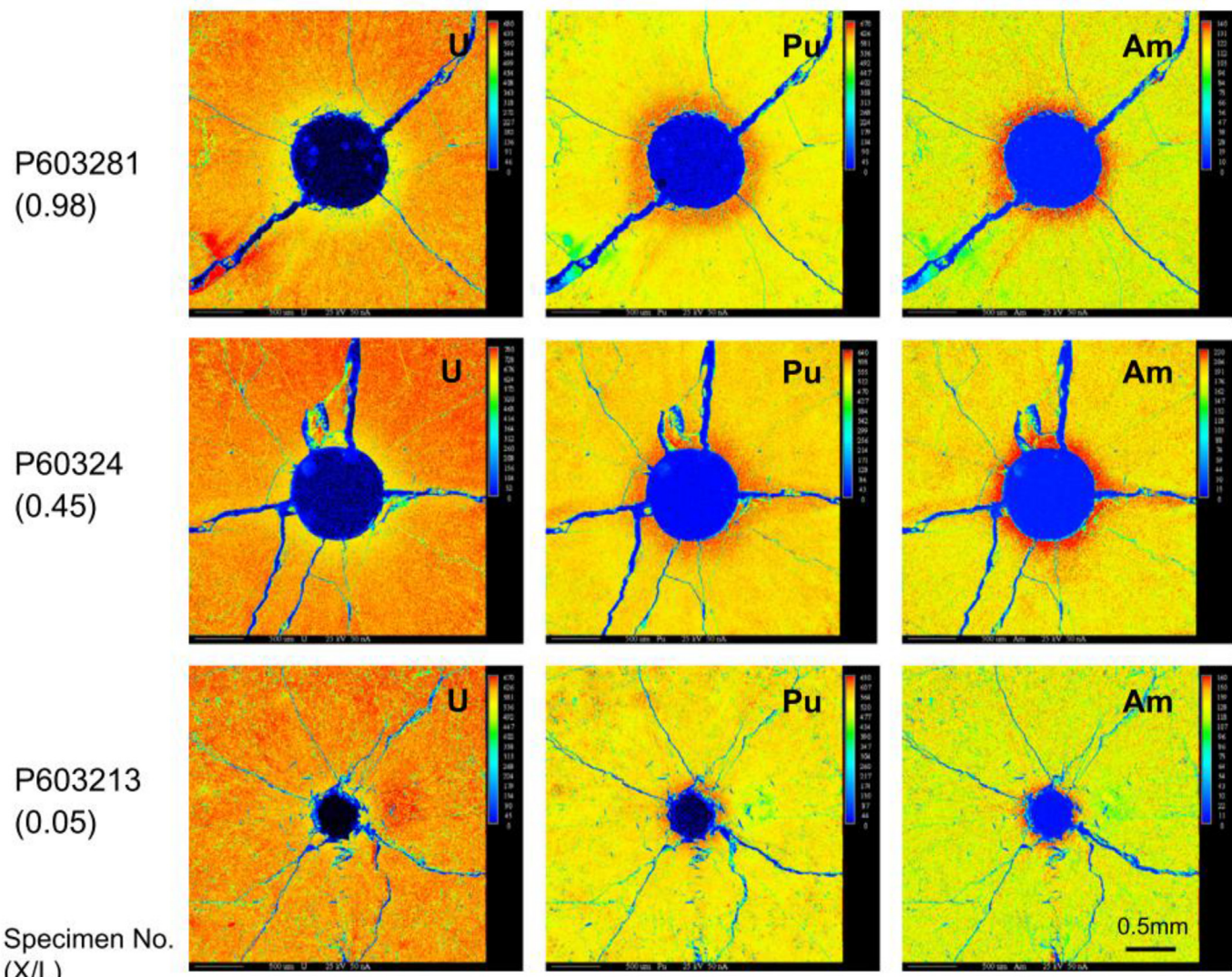


Fig. 5. EPMA X-ray maps of actinide redistribution of Am-doped MOX fuels irradiated for 24 h at 450 W cm^{-1} near the bottom (top row of figure), middle (center row), and top (bottom row) of the fuel rod length [29].

transport theory requires a higher number of cracks than those typically seen in thermally cycled fuels, while fission gas bubbles don't accumulate to large enough sizes at grain boundaries on the time scales considered.

Thermal diffusion is not believed to be the primary culprit of either of the discussed features, as it is a time dependent process that does not lead to any significant migration on short time scales of minutes or hours [17,18,22,23,25,28,31]. Fuel stoichiometry is the most widely observed and agreed upon fuel parameter leading to significant actinide redistribution [13,17–20,25–30,32,34,35,37–39]. Experimental results from several studies demonstrated that there is some threshold oxygen-to-metal (O/M) ratio in which the initial distribution of U and Pu in the fuel is retained [13,18,25,28]. While this threshold ratio varies as a result of factors such as centerline temperature and heating rate, the value tends to lie in the range of 1.96–1.97 O/M. At stoichiometries above the threshold value, Pu enrichment near the central void is to be expected, while a U enrichment is observed when the O/M ratio falls below the threshold. Fig. 6 provides a representative depiction of the effects of O/M ratio on the overall redistribution of actinides in MOX fuel following irradiation. High oxygen potentials create a higher partial pressure of UO_3 gas in the fuel system, with the U-rich species migrating to cooler regions of the fuel through the aforementioned pore evaporation-condensation process. This UO_3 migration ultimately leads to a U-depleted, actinide-rich region near the fuel centerline. Low oxygen potentials lead to the high volatility of the actinide based gaseous species, instead producing an actinide depletion near the central void [39]. It is important to note that the O/M ratio shifts over operating lifetime as heavy metal atoms fission into smaller lighter elements [18], creating an oxygen surplus within the fuel. At the time of this publication, there is little available quantitative data outlining the direct correlation between burnup and change in O/M ratio in fast reactor MOX fuel. A fraction of the newly unbounded oxygen will react with fission products or migrate to react with the cladding, but it is unknown at this time what effects mid-to-late life stoichiometry have on the actinide redistribution behavior.

4. Pu agglomerates

Referred to as Pu agglomerates (PA's), Pu-rich spots, or islands, regions of high Pu concentration form in the MOX fuel matrix. Due to the deviant behavior of the PA's during irradiation, clusters of

dispersed porosity form in the high Pu concentration regions. The overall appearance of the agglomerates varies with temperature and burnup of the region, displaying various morphologies dependent on the radial position [40–49]. Toward the outer, relatively cool section of the fuel, porosity forms small bubbles, only 1–2 μm in diameter, in high frequencies. In the intermediate radius of the pellet ($\sim 0.75 r_0 < r < 0.25 r_0$, where r is the radial position and r_0 is at the pellet edge), the densely populated, small pores start to agglomerate to form larger pores. Near the hot center of the fuel, the bubbles now reach sizes upwards of 50 μm with only a few isolated pores remaining. Fig. 7 shows the evolution of porosity formed in PA's at radial locations along the fuel pellet. Porosity formed due to PA's are visually distinct from those caused by fission gas accumulation on grain boundaries and porosity formed during pellet sintering. The pores are isolated and round in shape, in contrast to the irregular shaped interconnected porosity seen on grain faces in oxide fuels.

The porosity is formed as a result of highly localized burnup within the spots during reactor operation. PA's are highly dense in fissile material, with the high Pu content leading to heating rates and burnups beyond the low concentration UO_2 matrix material. Thermal conductivity of the spots is also lower than the surrounding grains [50], creating a space in which the agglomerates are simultaneously hotter and undergo a greater number of fission events in a very small region. Burnup in these regions may be greater than 2–3 times that of the pellet as a whole [43,51–55]. Electron probe micro-analysis (EPMA) studies following irradiation demonstrates the efficiency of burnup within these spots, showing reduction in overall Pu concentration of the spots by approximately 41% after 877 full power days and linear heating rates of approximately 250 W cm^{-1} [40].

High magnification examination of the pore surfaces reveals the presence of the high burnup structure (HBS) within the PA regions. While a more comprehensive review is available and recommended for further reading [53], a basic definition of the HBS structure can be defined as a fine grained, cauliflower-like structure (Fig. 8). In MOX fuels, the HBS structure appears in fuels following burnups between 60 and 80 GWd/tM at temperatures below approximately 1100 °C [42,43]. PA's reach these local burnups at pellet burnups far below this threshold, with the presence of the HBS ubiquitous in nearly all PA porosity. The overall morphology of the grains can evolve slightly depending on their location within the fuel [47]. In the outermost, cool region of the pellet, the grains remain incredibly fine, submicron sized grains on the order of 100–300 nm. Moving toward the center of the fuel, the HBS grains are annealed and begin to densify and grow, reaching sizes of approximately 1–5 μm around 1900 °C.

The formation of the spots is largely due to incomplete mixing and homogenization during the fabrication process. Several excellent articles exist that more thoroughly discuss the specifics of MOX fuel manufacturing [57–61], so the description given within the present review acts only to serve as a basic description of the underlying processes. Several routes exist for the production of modern MOX fuels, with the most commonly used being the micronized master (MIMAS) blend process. The process begins with the milling of PuO_2 powder with a UO_2 base, after which the milled powder is blended into a larger flow of UO_2 . MIMAS is commonly used due to the relatively low time, resource, and capital investment necessary for the process [62]. Only the starting (U, Pu) O_2 mixture requires ball milling rather than the entirety of the powder, potentially leading to uneven mixing of the powder. Early stages of MOX fuel development observed agglomerates on the order of 500 μm in diameter [63,64], but that number has steadily decreased to around 10–60 μm mean particle size and single digit volume fractions. The Pu concentration of the spots is determined

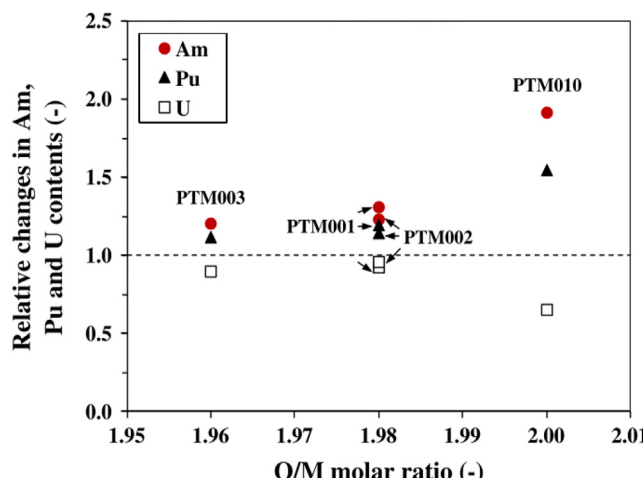


Fig. 6. Relative changes in U, Pu, and Am contents near the central void of the fuel pellet as a function of O/M ratio [13].

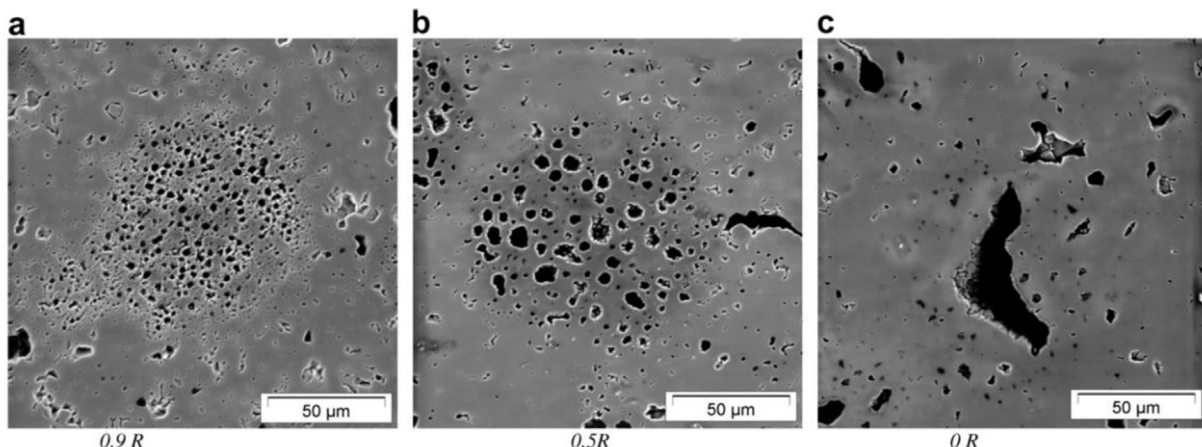


Fig. 7. Porosity formed in Pu agglomerates following irradiation as a function of radial position: a.) the pores near the outermost edge (0.9R, 90% of radius) of the pellet are small, but have a large frequency of spots, b.) the pores are slightly larger in the intermediate fuel diameter, and c.) the pores closest to the fuel center (0R, radius origin near central void) consist of a few, large pores [47].

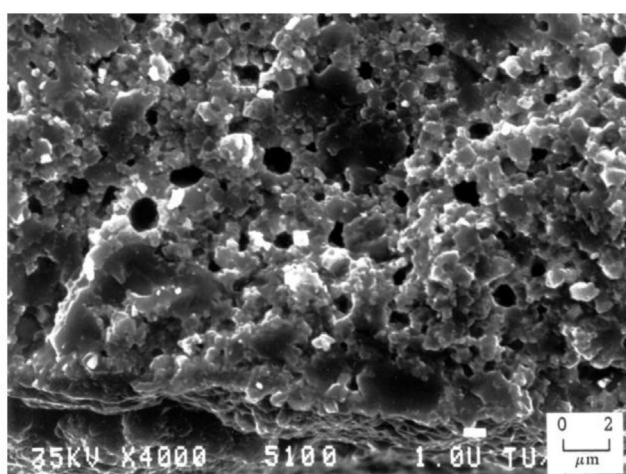


Fig. 8. Representative high burnup structure seen in high Pu content agglomerates, showing small, submicron sized grains surrounding porosity [56].

by the starting blend mixed into the UO_2 , but can reach as high as 45% PuO_2 [65]. PA's can be eliminated or reduced in size through more complete milling, powder sieving, or alternate fabrication, but agglomerates remain persistent in current MIMAS MOX fuel pellets. Detecting the spots has proven difficult to this point, with techniques capable of only detecting near surface agglomerates, or those larger than 500 μm in diameter [66–69].

Implications of PA's on overall fuel performance remain uncertain, but the prevailing consensus is that contribution to pellet burnup is minor. PuO_2 decreases the thermal conductivity when in solid solution with UO_2 , but the thermal conductivity of MOX fuels are much more dependent on the overall stoichiometry of the system rather than the contributions from discrete spots in the fuel [70–72]. Localized fuel swelling concerns exist as a result of solid fission products and fission gases implanted into adjacent grains, but the gases primarily accumulate along grain boundary pore networks, and swelling contribution of PA's is considered to have a minimal contribution to overall swelling behavior [41,43].

Agglomerates at the fuel-cladding interface are speculated to cause cladding perforation or failure during transient events [63,73]. However, this is only considered to be a possibility in the event of a particle several hundred micrometers in diameter being

directly in contact with the cladding and the event reaching temperatures high enough to eject molten Pu from the pellet. The presence of fuel surface PA's do have an impact on cladding oxidation behavior [43,45,46,73]. In the high burnup regions of the agglomerates, an excess of oxygen is created as a result of Pu fission, as the increased activity of oxygen in the region leads to an increase in oxide thickness in zirconium based cladding, [45]. Fig. 9 demonstrates this phenomenon, with the darker oxide region being definitively thicker than the layer visible toward the bottom of the image. This has shown no detrimental effect on structural integrity of the cladding, as the oxide layer is only 20–30 μm in thickness.

5. Solid fission products

Fission products are of great concern in nuclear fuel design due to the impact of the changing chemistry on fuel creep, swelling,

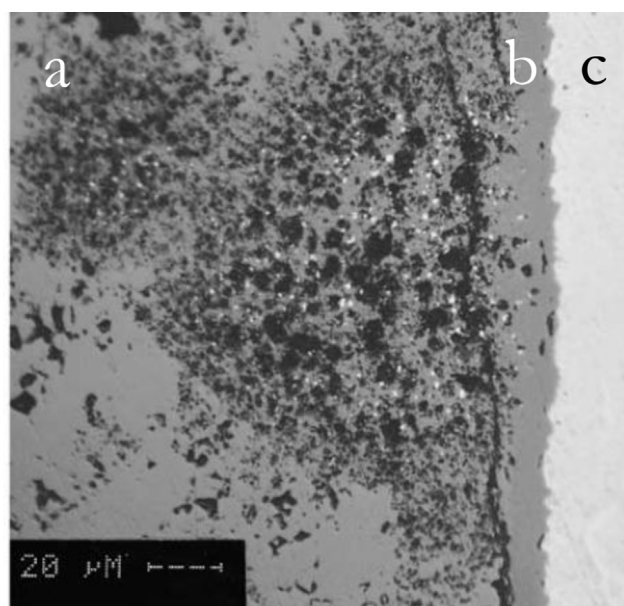


Fig. 9. Pu agglomerates (a) in 5.1 wt% PuO_2 MOX fuel near the fuel cladding interface at 42 GWd t^{-1} metal, demonstrating a thick cladding oxide layer (b) in the region near the agglomerates(cladding, c) [45].

thermal conductivity, and melting temperature. The chemical state of fission products in oxide fuels have been well understood since the mid-1980's, at which time Kleykamp [74] wrote the definitive review on the subject. In said review, the fission products are broken into 4 primary categories: fission gases and volatile species, metallic precipitate formers, oxide precipitate formers, and oxides formers that dissolve into the fuel matrix. The overall fission product yields of the U-235 and Pu-239 isotopes in MOX fuels are largely similar, but with several notable differences, as shown in Table 1. Pu-239 fission leads to a higher yield of metallic products like Ru, Rh, and Pd at the expense of oxide formers like Rb, Sr, Zr, and Y. While subtle, these differences do have an overall impact on the chemistry and distribution of the elements within MOX fuel pellets. The present review focuses on literature as it pertains directly to $(U, Pu)_O_2$ MOX fuels and only the predominant metallic precipitate and oxide precipitate phases. For a more thorough explanation and description of the total spectrum of fission products in oxide fuels, it is highly recommended that the reader consult the aforementioned review paper [74].

5.1. Metallic inclusions

While there are several minor metallic elements produced during the nuclear fission process, only Mo, Tc, Ru, Rh, and Pd form prominent phases in irradiated nuclear fuels. Commonly referred to as "white inclusions," "noble metal," or "five-metal" precipitates (Fig. 10), the particles exist as a solid solution taking on the hexagonal close packed (hcp) structure [74–82]. The particle size, frequency, and composition exist over a wide range, depending on the burnup and position found within the pellet. Mo and Ru are the highest concentration species, with descending concentrations of Tc, Rh, and Pd, respectively. In the columnar grain region of the fuel, the particles are commonly 5–10 μm in diameter [76,82–84], collecting primarily on the grain boundaries (Fig. 11a). The particles form as a result of fission product phase agglomeration, as opposed to nucleation and growth process. Particles tend to be much smaller (2 μm and below) [82,83] in the equiaxed and as-sintered regions, but occur more frequently either intergranularly or intragranularly (Fig. 11b).

At low burnups, the concentration of Mo in the metallic precipitates increases moving outward toward the pellet periphery, while Ru and Tc demonstrate the inverse behavior [16,76,77,83,85–88]. The relatively low yields of Rh show some minor response to radial position of the particles, but relatively little change occurs when compared to the other constituents. Pd

Table 1
Comparison of fission product yields from U-235 and Pu-239 irradiated using fast neutrons to 1% burnup after cooling for 1 year [74].

| Fission Product | Concentration (ppm) | | Fission Product | Concentration (ppm) | |
|-----------------|---------------------|--------|-----------------|---------------------|--------|
| | U-235 | Pu-239 | | U-235 | Pu-239 |
| Kr | 120 | 60 | Sn | 32 | 35 |
| Rb | 130 | 60 | Sb | 14 | 14 |
| Sr | 260 | 100 | Te | 140 | 170 |
| Y | 180 | 60 | In | 80 | 100 |
| Zr | 1000 | 650 | Xe | 1050 | 1150 |
| Nb | 7 | 7 | Cs | 960 | 950 |
| Mo | 890 | 790 | Ba | 390 | 310 |
| Tc | 220 | 210 | La | 290 | 260 |
| Ru | 480 | 800 | Ce | 690 | 630 |
| Rh | 130 | 230 | Pr | 340 | 260 |
| Pd | 110 | 580 | Nd | 980 | 870 |
| Ag | 8 | 80 | Pm | 90 | 110 |
| Cd | 8 | 35 | Sm | 140 | 220 |
| In | 1 | 4 | Eu | 20 | 40 |

metal has the highest vapor pressure [88] of the white inclusion components and migrates outward toward the cladding. Pd rich phases are commonly found on the outer rim of the fuel, which may include any of Cs, Te, Sn, Ag, or fissile U or Pu [86], or deposited directly on the cladding surface [89,90]. There are instances in which additional body-centered cubic (BCC) or face-centered cubic (FCC) phases can form from the metallic products due to local composition effects [77,78,91], but these phases are minor in comparison to the noble metal precipitates.

The amount of Mo available for metallic precipitates is dependent on the oxygen potential inside the fuel. It is more favorable for the noble metals to remain metallic in the temperature ranges seen during irradiation [76]. Mo, being multivalent, can either be metallic or form an oxide, depending on the oxygen available in the system. In hypostoichiometric fuels where the O/M ratio is below approximately 1.98, the Mo is primarily in the metallic state [78,92]. As the fission process proceeds and fissile material releases its bound oxygen, the oxygen potential of the system increases [93,94]. The effects of burnup and increased oxygen potential on the concentration of Mo in the metallic precipitates in the columnar grain region is clearly demonstrated in Fig. 12. Near 7% burnup, the Mo content of the inclusions drops dramatically [87], likely due to the excess of available oxygen within the system. While cladding oxidation and oxide forming precipitates do get a small amount of the available oxygen, the potential of the system is still above the threshold O/M limit. Mo can form several byproducts, including MoO_2 to incorporate into other oxide fission products, MoO_3 , or react with Cs to form Cs_2MoO_4 .

5.2. Oxide phases

When compared to the white inclusions mentioned previously, the literature available for direct studies of oxide precipitates forming in MOX fuels is relatively limited. Oxides containing Sr, Zr, or the rare earth (RE) elements form solid solutions with either UO_2 , PuO_2 , or both at low concentrations [95]. Barium is only soluble to 1.6 at% at 1450 °C in 20 wt% PuO_2 MOX fuels and thus precipitates a separate oxide phase at higher concentrations [96]. These oxides, commonly referred to as the "grey phase," form ABO_3 perovskite structures, in which A = $(\text{Ba}_{1-x-y}, \text{Sr}_x, \text{Cs}_y, x, y \ll 1)$ and B = (U, Pu, Zr, Mo, RE) [91]. Due to the sheer number of possible constituents in the phase, it is difficult to pinpoint a typical composition, but reported data suggests that the particles are primarily Ba rich, followed by Zr, U, Pu, Mo, Sr, and trace amounts of the remaining products in descending order of wt% [16,91,97]. Grey phase is typically found in the equiaxed or outermost regions of the columnar grains [16,96,97], commonly intermixed with other constituent oxides as shown in Fig. 13.

5.3. Impact on fuel performance

Several studies have been conducted on the thermophysical properties of the metallic and oxide fission products, or other suitable model systems [80,98–104]. As would be expected, the white inclusion alloys display much higher thermal conductivity than the oxide fuel or grey phase, creating the potential for hot spots within the matrix or localized melting of the particles during transient events [80]. Grey phase perovskites of the form BaUO_3 or BaPuO_3 have demonstrated thermal conductivities much lower than that of UO_2 [99,105], reported to be as low as one tenth the value of the fuel matrix at room temperature [105]. Oxides may form low temperature eutectics with the fuel matrix, again leading to concerns regarding localized melting [106].

The greatest concern regarding the impact of fission products on MOX fuel performance is the depression of the fuel melting point as

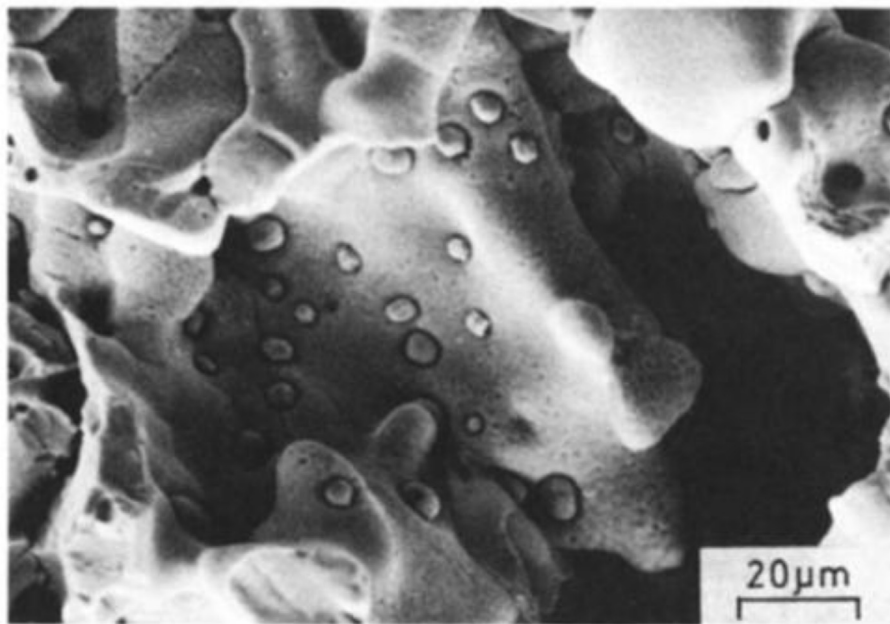


Fig. 10. Secondary electron image of metallic inclusions in irradiated FBR MOX fuel pin [162].

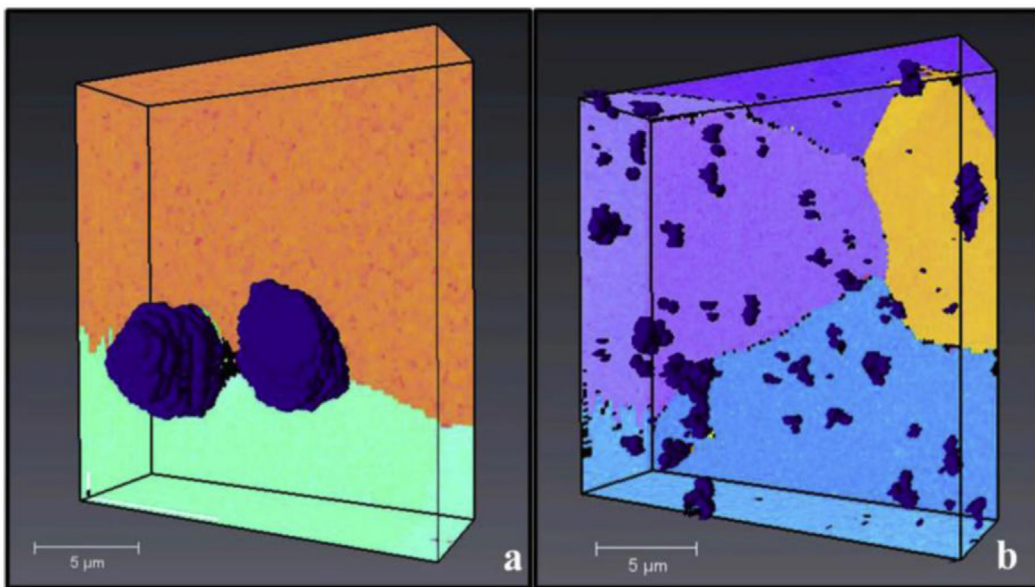


Fig. 11. 3D electron backscatter diffraction (EBSD) reconstructions of 6.7% FIMA MOX fuel showing a.) large intergranular metallic precipitates in the columnar grain region and b.) small inter- and intragranular metallic precipitates near the pellet periphery [82].

burnup increases. Fuels see a reduction in melting temperatures between 20 and 30 °C, depending on initial composition and burnup of the fuel in use [106,107]. Issues with localized hot spots and incipient melting are primarily introduced when directly in contact with fuel cladding, potentially corroding or oxidizing the rods. While it is useful to understand the specific properties of each solid fission product, the volume fraction of each product category is very small compared to the amount fissile material, even at very high burnups. There is no singular solid fission product that directly leads to the overall shift in MOX fuel properties, but rather an intricate interaction between each of the constituents that alters the fuel performance over the reactor lifetime.

6. Joint-Oxide Gain

The volatiles class of fission products produced during reactor operation are of particular interest as they pertain to the peripheral structures created by FCCI [108], fuel-cladding mechanical interaction (FCMI) [109], and the pellet-cladding gap [87]. Products like Cs, Te, and I all evaporate at low operating temperatures and migrate to the coolest part of the fuel assembly where they react with fuel or cladding constituents. As stated previously, the behavior of Mo varies largely based on the O potential of the fuel. As such, it has a tendency to combine with Cs and O to become volatile and migrate toward cooler fuel regions. Tourras et al. [87] were the

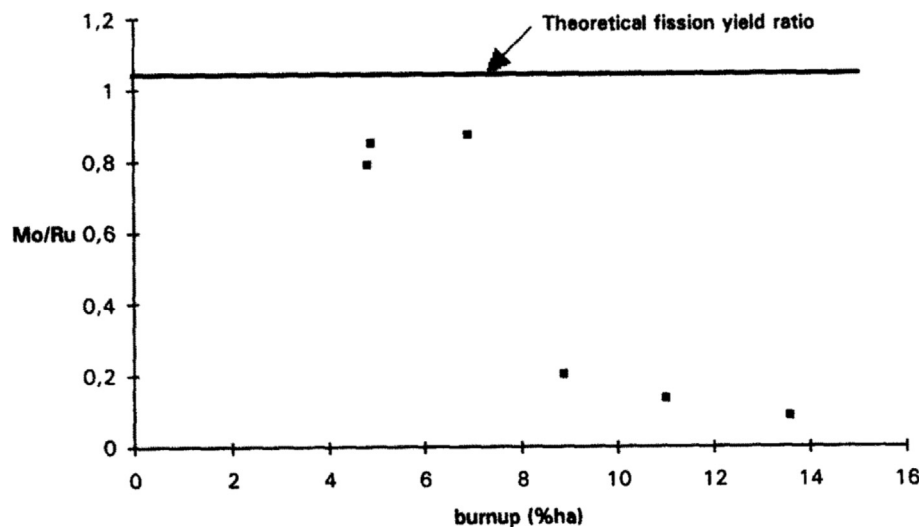


Fig. 12. Mo/Ru ratio of noble metal precipitates in the columnar grain region shown as a function of burnup in 20 wt% PuO₂ MOX fuels [87].

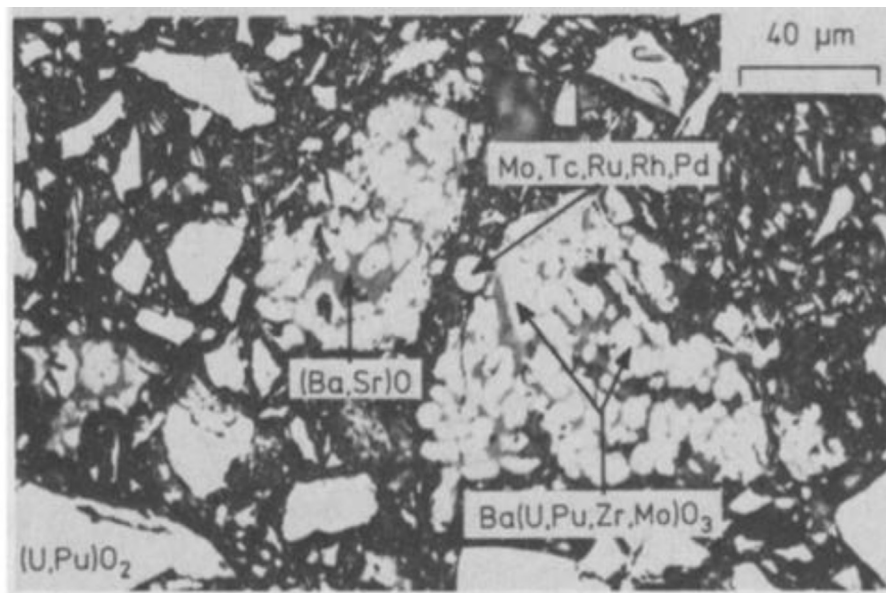


Fig. 13. Microstructure of irradiated FBR fuel pins displaying the mixture of oxide fuel, white inclusions, and grey phase [77].

first to name JOG, or “Joint-Oxide Gain” referring to an oxide buildup formed on the fuel surface between the pellet and cladding in PHENIX fuel pins. Consisting primarily of Cs₂MoO₄ or Cs₂(U, Pu)O₄, the JOG structure is irregular and dense, found in regions where the peak fuel temperature is lowest [87,89,90,109–111]. The volatile constituents of the JOG structure evaporate from the fuel pellet at high temperatures and condense to become solid at the cooler top or bottom of the fuel assemblies. Fig. 14 shows an energy dispersive X-ray spectroscopy (EDS) map of the constituents of the JOG region, with Cs and Mo clearly showing the highest intensity in the JOG region. JOG has a threshold burnup of formation between 70 and 90 GWd/t [87,89,112], at which point the fuel-cladding gap increases along with the thickness of the JOG structure. This behavior is attributed to the reduction in fuel swelling, as fission products incorporated into the fuel matrix are expelled and become available to react at the pellet edge.

Literature on direct observations of JOG structure are relatively

sparse, with far greater interest on the ability to model the effects on fuel performance. The thermal conductivity of Cs₂MoO₄ varies based on the temperature regime it is operating in, as well as the overall density of the structure. At low temperatures, the structure exists in the orthorhombic phase in which the thermal conductivity decreases with increasing temperature [113–116]. Above approximately 570 °C, it undergoes a phase transition to a hexagonal structure that shows an increase in thermal conductivity at high temperatures. JOG density shows a linear relationship to the thermal conductivity, with highly dense structures having higher thermal conductivity [114]. Several studies [113–117] on the thermal properties of Cs-Mo-O and Cs-(U, Pu)-O structures have demonstrated that the thermal conductivities of both compounds are 5–10% that of UO₂ base fuel [115]. However, it is believed that the existence of JOG aids in thermal transport of the fuel, as the oxide structures have higher thermal conductivity than a fuel-cladding gap filled with fission gases. Modelling efforts to

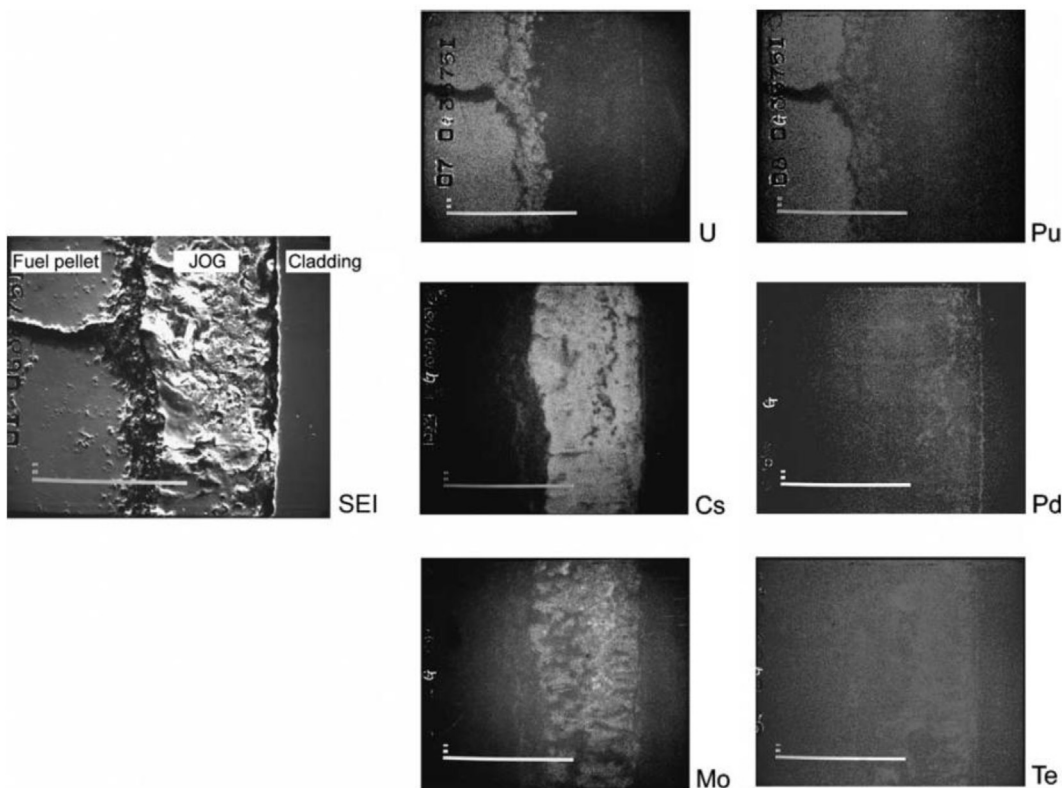


Fig. 14. X-ray mapping of 30 wt% Pu MOX fuel-cladding gap including JOG region near the fuel pin mid-position with a local burnup of 127 GWD t^{-1} [123].

incorporate the presence of JOG into fuel performance codes agree with the conclusion, with the JOG presence leading to a decrease in overall temperature of simulated MOX fuel pins [118–122].

7. FCCI

FCCI is a complex phenomenon that has been reviewed recently by Maeda [124] in much greater detail than will be discussed in the present work. This review will largely summarize the major points outlined in Maeda's work, and as such, it is highly recommended that the reader consult the said review for a more complete description of FCCI properties. As FCCI formation is a thermally driven process, it is important to note that the following phenomena pertain to fast reactor MOX systems [125]. The cladding inner surface temperature of LWR MOX fuels do not reach sufficiently high temperatures under normal operating conditions to initiate detrimental oxidation and chemical attack. The greatest concerns regarding FCCI and its impact on reactor operation involves potential failure and breach of fuel cladding in which the coolant interacts with the fuel directly. Penetration depth and cladding wastage are key parameters of FCCI formation that dictate the likelihood of such an event occurring. FCCI manifests itself in three primary modes: matrix attack, intergranular attack, or combined, which demonstrates the properties of both matrix and intergranular attack [125]. Matrix FCCI attack (Fig. 15b) corresponds to the localized oxidation of the cladding material [126], with primarily oxidation of the Cr in the stainless steel. Intergranular attack (Fig. 15a) modes occur due to the depletion of Cr in grain boundaries due to the formation of Cr_{23}C_6 carbides allowing penetration of corrosive species [127].

Oxygen and volatile fission products (Cs, Te, I, etc.) are the primary culprits of FCCI initiation in oxide fuel systems. In Pu bearing MOX fuels, the oxygen potential of the system is the greatest

difference from UO_2 , as the preferential formation of noble metals rather than oxide formers leads to an excess of available oxygen in the system. Oxygen is a primary driver in the formation of the FCCI, as it leads to oxidation of the cladding and volatiles. Under normal operation, stainless steel cladding forms a chrome oxide (Cr_2O_3) layer that acts to protect the cladding from corrosion. In its elemental form, Cs is unreactive with stainless steel claddings, but reacts with the protective oxide layer to create Cs-chromates [128] (Cs_2CrO_4 or $\text{Cs}_2\text{Cr}_2\text{O}_7$) when excess oxygen is present. The decay of the protective oxide layer causes deeper penetration of the FCCI into the cladding. Iodine is primarily bound to Cs in the form of CsI, which is non-corrosive in said state [128]. It can, however, lead to an enhancement in oxidation in hyperstoichiometric fuels. Tellurium is highly active when combined with Cs to create Cs_2Te [129], a compound that can dissolve cladding constituents in the presence of high oxygen potential.

Several empirical models [125,126,130–132] have been developed with the purpose of predicting the interaction depth of FCCI formation. While each model has unique constants and weighting for parameters, there are several key aspects of the fuel that are included in every approximation. The O/M ratio of the fuel before and during irradiation are significant factors, as excess oxygen in the system increases the rate of cladding attack [133]. By using hypostoichiometric fuels with an O/M ratio of <1.96 , oxygen redistribution during irradiation results in an O/M ratio at the surface of less than 1.996, at which point excessive oxidation of the Cr in the stainless steel cladding will not occur [133]. As stated previously though, oxygen is significant in the facilitating role for chemical attack from volatile fission products. Fuel burnup is another primary consideration, as it produces the volatile fission products that induce chemical attack. As a result, there is a direct relationship between burnup and FCCI cladding depth [125]. Cladding temperature and the temperature gradient between the

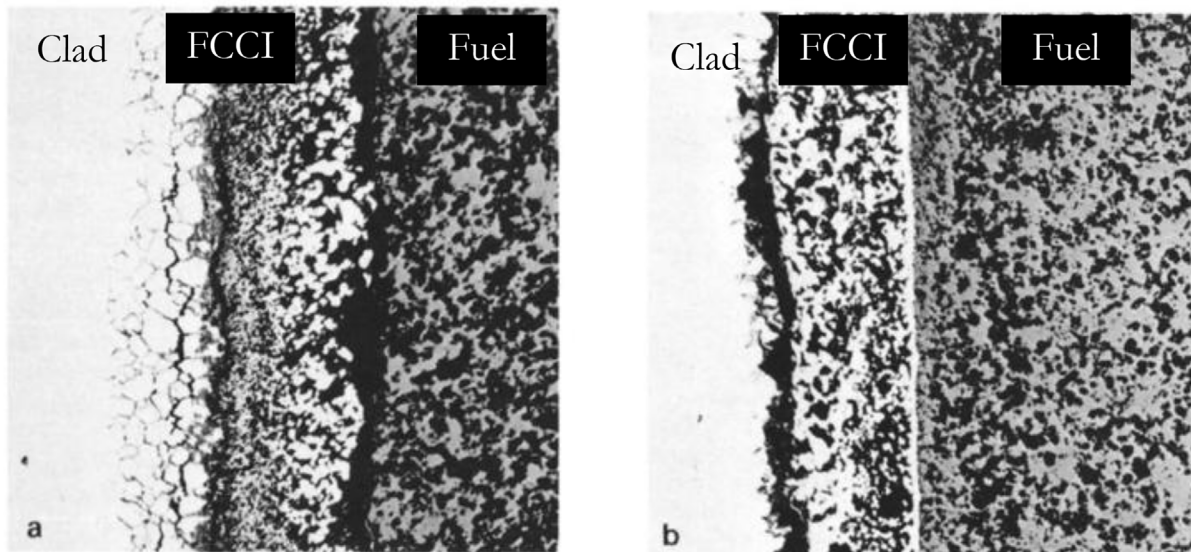


Fig. 15. Micrograph of FCCI layer in 20 wt% PuO₂ MOX fuel clad with stainless steel showing a.) intergranular attack, and b.) matrix attack [128].

fuel and cladding both have significant impact on FCCI formation as well. Stainless steel becomes susceptible to chemical attack near 500 °C [127], and the experimental evidence shows there is a distinct onset of FCCI near this temperature [126,128,134].

8. Recent research trends

Experimental MOX research has been an active field within the last decade. Two notable categories stand out as the most prominent fields in fuel analysis in the time period from 2008 to 2018. The first major research thrust is a reexamination of the thermal properties of MOX fuels. The thermophysical properties of (U,Pu)O₂ fuels have been extensively analyzed since the 1960's, but additional information and refinements are still being performed today. As MOX fuels attempt to push toward higher burnups and higher Pu concentrations for efficient Pu elimination in fast reactors, a thorough understanding of the fuel thermal behavior is crucial for safe reactor operation. Kato et al. [135,136] cited discrepancies in early work determining the solidus and liquidus temperatures of (U, Pu) O₂ MOX fuels of approximately 40 mol% Pu due to fuel interaction with the tungsten heating filament used for the experiment. By substituting a less reactive rhenium vessel with the tungsten container, they discovered that the solidus temperature is approximately 100 K higher than initially reported for 40% Pu MOX fuel (Fig. 16) [135]. Additional systematic studies to determine the effects of burnup [71,72,137,138], O/M ratio [139–144], Pu fraction [143,145,146], and oxygen potential [143,147] on thermal and chemical properties of MOX fuels have been recently performed. This approach is necessary for the development of fuels tailored to the exact properties necessary for efficient reactor operation and has been a missing component through the decades of fuel development.

The second major research area of the last ten years has been on the impacts of incorporating minor actinides (MA's) on fuel behavior. MA's (americium, neptunium, curium, etc.) make up a small volume fraction of the overall waste fuel, but are responsible for approximately 33% of the overall activity [148] when in long term storage. By recycling both Pu and the MA's, the amount of time necessary for fuel waste to fall below the radiotoxicity level of uranium ore drops from millions of years to hundreds [149].

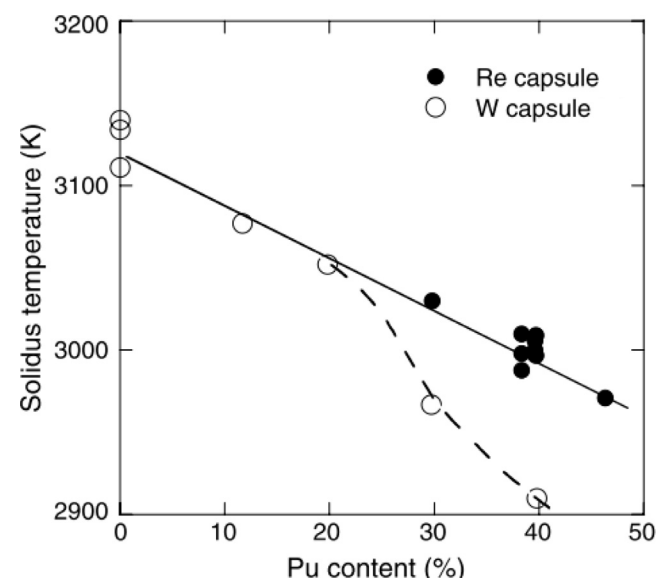


Fig. 16. Comparison of solidus temperature of UO₂ as a function of Pu content comparing results obtained with Re and W capsules [135] (data for W capsule from Ref. [136]).

Thermal conductivity decreases 1–2.5% at temperatures below 1300 K, but these effects are negligible at higher temperatures [150,151]. Neptunium has a lower impact on thermal properties [150,151] when compared to Am containing fuels, as the lattice mismatch between the base fuel is low and thus phonon scattering is lessened. MA redistribution in the columnar grain region follows the same principles as Pu in pure MOX fuels, with the O/M ratio again being the determining factor [27–29,152]. Americium accumulation near the central void is more pronounced with increases in concentration around the central void of 30–50% following 24-h irradiation [27–29,152], while Np has shown no notable propensity to redistribute [28]. Fig. 17 shows the radial profiles of Am, Np, and Pu, demonstrating the clear redistribution of Pu and Am with no noticeable changes in Np concentration near the central void.

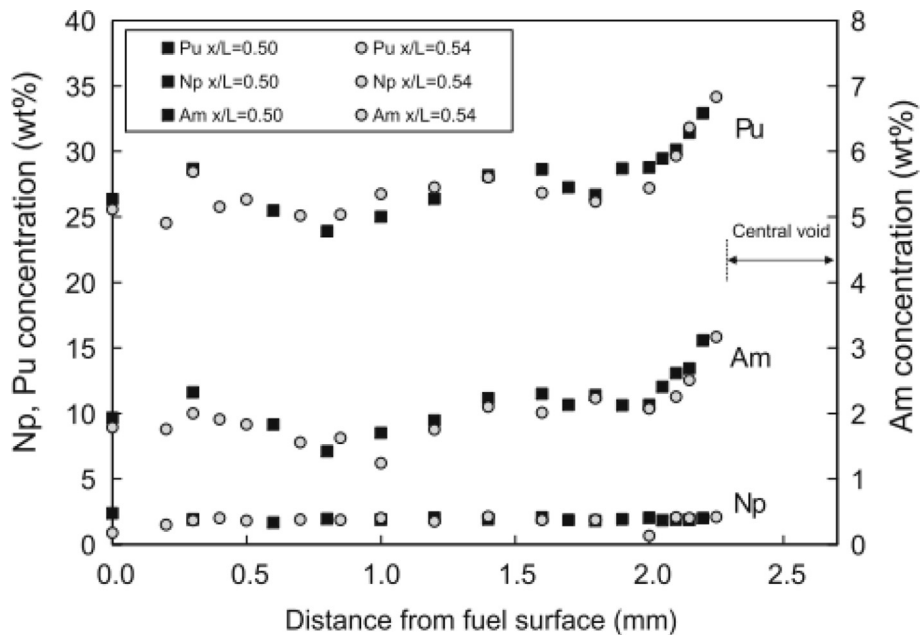


Fig. 17. Radial profiles of Am, Np, and Pu for $(U_{0.672}Pu_{0.288}Am_{0.020}Np_{0.020})O_{1.98}$ MOX fuel irradiated for 24 h at a LHR of 430 W cm^{-1} [28].

9. Summary of research outcomes to date

As it has been noted in this review article, a significant amount of work has been conducted to study fuel structuring and Pu redistribution, Pu agglomerates, fission product chemistries, JOG formation, and FCCI in MOX fuels. From the available literature, the following conclusions can be drawn:

1. O/M ratio is one of the most significant factors in determining the nature of actinide redistribution, fission product precipitate chemistries, and FCCI formation.
2. The effects of fission product precipitates and Pu agglomerates on fuel thermal behavior is highly localized with little discernible influence on the overall fuel burnup behavior.

Current MOX fuel development is aiming to make the fuel highly versatile in order to burnup large amounts of Pu and transuranic species otherwise deposited in long term storage. Therefore, fuels must be able to operate up to high burnup states with Pu loading in the range of 30–40 wt%. In order to do this, it is necessary to understand the long term evolution of nuclear fuels up to said threshold and beyond. A comprehensive understanding of fuel microstructures and properties is necessary for safe and efficient operation, requiring a thorough understanding of fuel behavior at each point in the fuel life cycle. Several areas of improvement have been identified based on the conducted literature review and recommendations for filling the knowledge gap suggested.

10. Areas of improvement

Fundamental understanding of fuel behavior requires in-depth analysis across a wide range of length scales. Radiation creates defects at an atomic level, giving rise to defects of 0D (vacancies and interstitials), 1D (dislocations and dislocation loops), 2D (fuel-fission product interfaces and restructured grains), and 3D (voids, cracks, precipitate fission product phases) scales. The accumulation of point defects caused by neutron irradiation ultimately leads to the formation of higher order defects, making the comprehension of atomic and nanoscale characteristics crucial to the

understanding of fuel evolution. Features of this size scale could not be observed due to the limited availability of the tools necessary for imaging at the time of research. Access to advanced imaging technology, such as transmission electron microscopes (TEM) and focused ion beams (FIB) instruments, has historically been restricted for highly radioactive materials. However, infrastructure investments by national laboratories and universities has made the nanoscale data readily available to supplement and enhance the previous 60 years of MOX fuel understanding.

The development of microstructure-properties relationships is especially important for the safety and efficiency of MOX fuel reactor operation, owed to the highly localized nature of the fuel microstructures. As a fundamental tenet of materials science, the microstructure and chemistry of the material will dictate the physical properties. The columnar, equiaxed, and as-sintered regions of restructured MOX fuel pellets have unique microstructures and will display varying thermo-physical behaviors. Property measurements primarily describe bulk material response with little consideration for the individual phases, but contributions from the constituent phases evolve with increasing burnup and must be accounted for.

Tools for measuring the properties of individual phases are becoming readily available for use in the nuclear community. The diameter of fission product phases and FCCI interaction zone thicknesses are 10's of microns or smaller, making nanoindentation an ideal technique to isolate the hardness, modulus, and creep parameters of a single grain or precipitate from the bulk. In-situ nano-mechanical testing systems mounted in SEM and dual-beam FIB systems have begun to gain traction in testing structural reactor materials [153,154] and fresh fuels [155], but little-to-no data has been published on the measurements obtained from neutron irradiated fuels. In-situ systems offer the benefit of being enclosed in a microscope chamber in which additional shielding may be used to protect the tool operators from excess exposure, while the phase selectivity of the tool is a major selling point of the technique. State-of-the-art models have high temperature capabilities (up to approximately 800°C) for property measurements near reactor operating conditions.

Thermal transport in nuclear fuel is the most important

property during irradiation, as it is the entire basis for energy production. However, that heat must move across boundaries and phases that are constantly evolving during the burnup process. Hurley et al. [156] are working to develop a tool to directly measure the thermal conductivity and diffusivity of irradiated fuels using a photothermal reflectance technique. The "Thermal Conductivity Microscope" would allow for the collection of thermal properties on size scales consistent with MOX fuel features. Additionally, the tool could be used to safely examine highly radioactive material at a variety of temperatures. Techniques such as this will provide a pathway toward comprehension of the overall contribution of sub-micron features to the bulk behavior of nuclear fuels.

With new capabilities and design goals in mind, it is also necessary to develop a thorough comprehension of the true structure of materials. While it is convenient to depict and describe materials in 2D, it is important to remember that all materials exist in 3D. Traditional imaging techniques such as optical, scanning electron microscopy (SEM), and TEM techniques are relegated to 2D characterization of materials, which has been sufficient for base level understanding of material microstructure. TEM is a valuable tool for its high resolution imaging capabilities, but the overall volume of material examined from a single specimen cannot be considered representative of an entire fuel pellet. TEM lamella prepared using a FIB tool have a volume of approximately $10 \mu\text{m}^3$ (assuming lamella are $10 \mu\text{m}$ tall, $10 \mu\text{m}$ wide, and 100 nm thick). Dozens of TEM lamella must be analyzed to describe the highly variable microstructure of a single fuel pin cross-section, a time-consuming process in which the micrographs still do not provide morphological descriptions. EDS information collected during TEM has additional difficulties as it relates to uranium and transuranic analysis. Energy peak overlap for U, Pu, and Am makes EDS resolution exceptionally difficult and standards for these elements are commercially unavailable.

Non-destructive examination tools, such as X-ray tomography, neutron radiography, and synchrotron source experiments, are capable of creating 3D reconstructions of nuclear fuels to examine relatively large volumes of materials, but lack nanoscale resolution. Many of the large volume analysis tools rely on phase contrast to determine the size and shape of phases, but do not have the means to identify the chemical composition of unknown phases. Destructive, high resolution techniques like atom probe tomography (APT) and secondary ion mass spectroscopy (SIMS) provide atomically sensitive chemical and morphological data, but again suffer from the issues associated with statistically significant materials volumes. Neither technique has been extensively utilized in oxide fuel analysis. APT has recently adopted the advanced laser technology necessary for ceramic analysis, but the volume of material analyzed again requires dozens of samples to demonstrate representative fuel behavior [157]. SIMS analysis can provide detailed insight into the isotopic and chemical nature of nuclear fuel, but the highly surface sensitive nature of the technique effectively relegates analysis to 2 dimensions [158]. 3D characterization techniques must be able to effectively cover the mesoscale gap with the submicron resolution necessary for comprehensive structure descriptions.

Along with standard postirradiation examination (PIE), much of the computational work to date on microstructural evolution during reactor operation has been constrained to 2D materials systems. With the advent of new materials modelling codes such as the Multiphysics Object Oriented Simulation Environment (MOOSE) and its accompanying packages, predictive modelling in nuclear fuels and materials through direct microstructure incorporation is now readily available. Irradiated fuels are highly complex systems with evolving microstructures and chemistries. As a result, the properties of the fuel will be dictated by the stage of the burnup

process. The direct incorporation of 3D microstructures into the MOOSE framework allows for truly predictive simulation capabilities, ultimately opening the possibilities for accurate materials-properties relationship descriptions based on actual MOX fuel responses at escalating stages of operation. Through the iterative improvement of experimental validation of the computational models, rapid and safe deployment for advanced MOX systems is possible for next generation reactor technologies.

Recent work by Teague and Tonks et al. [82,159–161] has been performed as a proof-of-concept addressing the issues associated with statistically significant sample size and experimentation-modelling validation. FIB tomography is a technique that has gained a great deal of attention since the early 2000's with the advancement of slice-and-view automation and FIB reliability. FIB tomography has the benefit of analyzing relatively large material volumes ($\sim 50 \mu\text{m} \times 50 \mu\text{m} \times 50 \mu\text{m}$) with high resolution ($\sim 10 \text{ nm}$). When paired with EDS and EBSD, micrographs encapsulating phase morphology, chemistry, and crystallographic orientation are collected in a single scanning step. Teague and Tonks [161] were able to directly import the 3D microstructure of irradiated MOX fuels into the MARMOT materials simulation code to predict the thermal properties at varying radial fuel positions.

Through careful planning, collaborations similar to the previously mentioned approach have the potential to rapidly improve next-generation materials modelling capabilities. Open communications between the computational and experimental communities must improve in order to effectively gather the data needed by both parties in order to fully realize the potential of predictive modelling in nuclear materials. Both groups must develop a common understanding of the language used by the other to concisely describe the inputs needed for the model generation and validation. An in-depth understanding of the limitations of the techniques needs to be clearly outlined from the inception of the project with clear goals and key outcomes stated outright.

11. Recommendations

The following approaches for future MOX fuel and nuclear materials research are suggested:

1. Develop a fundamental understanding of MOX fuels at the nano-scale. Radiation induced point defects agglomerate to form higher order defects, so understanding the basic motion of vacancies, interstitials, and dislocations during irradiation will provide insights into the macroscale fuel response. TEM and atom probe tomography are among the techniques necessary to provide nanoscale analysis of the irradiated MOX fuel response.
- 2 Adapt 3D characterization techniques to provide an accurate description of MOX fuel microstructure and analyze statistically significant volumes of material. MOX fuel has been examined extensively at the macroscale, so supplementing this data along with the aforementioned nanoscale analysis will lead to more complete MOX fuel examination. The greatest difficulty associated with this sort of analysis will likely be the time necessary to collect the data. High resolution imaging is a time intensive process and the problem is magnified when applied to large sample sizes, though improvements in equipment and detector efficiencies will likely mitigate this issue as the technology matures. Techniques like FIB tomography are more readily available and accessible for irradiated materials, with the operation becoming largely automated to assist in timely data collection. The standardization and optimization of experimental methods for these techniques will also be necessary to the future success of this analysis.

3 Build collaborative computational models using experimentally gathered microstructures to improve the predictive capabilities of the simulation tools. Computational models are capable of incorporating microstructural features across length scales to predict the thermo-physical properties of materials systems. An experimental-computational feedback loop to validate the models will provide simultaneous benefits to both parties, ultimately moving toward a highly advanced predictive model to improve reactor safety and efficiency. It is critical to encourage open communication between computational and experimental scientists to ensure that the type and quality of data collected is useful for code incorporation. Providing microstructural and chemical data sets from experimental works will directly improve the accuracy of the computational models to decrease the time from inception to implementation for new fuel concepts. Creating an open access database of collected data would provide a highly valuable resource to code developers to test new ideas and ultimately work to predict structure-properties relationships, which will in-turn be validated through experimental means.

References

- [1] D.C. Crawford, D.L. Porter, S.L. Hayes, Fuels for sodium-cooled fast reactors: US perspective, *J. Nucl. Mater.* 371 (2007) 202–231, <https://doi.org/10.1016/j.jnucmat.2007.05.010>.
- [2] S.J. Zinkle, G.S. Was, Materials challenges in nuclear energy, *Acta Mater.* 61 (2013) 735–758, <https://doi.org/10.1016/j.actamat.2012.11.004>.
- [3] F. Delage, J. Carmack, C.B. Lee, T. Mizuno, M. Pelletier, J. Somers, Status of advanced fuel candidates for sodium fast reactor within the generation IV international forum, *J. Nucl. Mater.* 441 (2013) 515–519, <https://doi.org/10.1016/j.jnucmat.2012.09.036>.
- [4] J.J. Carbajo, G.L. Yoder, S.G. Popov, V.K. Ivanov, A review of the thermo-physical properties of MOX and UO₂ fuels, *J. Nucl. Mater.* 299 (2001) 181–198.
- [5] A. Ishimi, K. Katsuyama, Y. Kihara, H. Furuya, Fuel performance of hollow pellets for fast breeder reactors, *J. Nucl. Sci. Technol.* 53 (2016) 951–956, <https://doi.org/10.1080/00223131.2015.1085337>.
- [6] J.D.B. Lambert, R. Strain, Oxide fuels, in: R.W. Cahn, P. Haasen, E.L. Kramer (Eds.), *Mater. Sci. Technol. A Compr. Treat.*, WILEY-VCH Verlag GmbH & Co KGa, 1994, pp. 109–190.
- [7] C. Sari, Grain growth kinetics in uranium-plutonium mixed oxides, *J. Nucl. Mater.* 137 (1986) 100–106.
- [8] C.N. Venkiteswaran, V.V. Jayaraj, B.K. Ojha, V. Anandaraj, M. Padalakshmi, S. Vinodkumar, V. Karthik, R. Vijaykumar, A. Vijayaraghavan, R. Divakar, T. Johny, J. Joseph, S. Thirunavakkarasu, T. Saravanan, J. Philip, B.P.C. Rao, K.V. Kasiviswanathan, T. Jayakumar, Irradiation performance of PFBR MOX fuel after 112 GWD/t burn-up, *J. Nucl. Mater.* 449 (2014) 31–38, <https://doi.org/10.1016/j.jnucmat.2014.01.045>.
- [9] K. Tanaka, S. Miwa, I. Sato, T. Hirosawa, H. Obayashi, S. Koyama, H. Yoshimochi, K. Tanaka, Microstructure and elemental distribution of americium-containing uranium plutonium mixed oxide fuel under a short-term irradiation test in a fast reactor, *J. Nucl. Mater.* 385 (2009) 407–412, <https://doi.org/10.1016/j.jnucmat.2008.12.028>.
- [10] F. a Nichols, Theory of columnar grain growth and central void formation in oxide fuel rods, *J. Nucl. Mater.* 22 (1967) 214–222, [https://doi.org/10.1016/0022-3115\(67\)90031-1](https://doi.org/10.1016/0022-3115(67)90031-1).
- [11] K. Katsuyama, T. Nagamine, S.I. Matsumoto, M. Ito, Measurement of central void diameter in fbr mox fuel by x-ray computer tomography, *J. Nucl. Sci. Technol.* 39 (2002) 804–806, <https://doi.org/10.1080/18811248.2002.9715263>.
- [12] K. Katsuyama, K. Maeda, T. Nagamine, H. Furuya, K. Katsuyama, K. Maeda, T. Nagamine, Three-Dimensional x-ray CT image of an irradiated FBR fuel assembly, *Nucl. Technol.* 169 (2010) 73–80, <https://doi.org/10.13182/NT10-A9344>.
- [13] K. Maeda, K. Katsuyama, Y. Ikusawa, S. Maeda, Short-term irradiation behavior of low-density americium-doped uranium-plutonium mixed oxide fuels irradiated in a fast reactor, *J. Nucl. Mater.* 416 (2011) 158–165, <https://doi.org/10.1016/j.jnucmat.2010.11.027>.
- [14] M.V. Speight, The migration of gas bubbles in material subject to a temperature gradient, *J. Nucl. Mater.* 13 (1964) 207–209, [https://doi.org/10.1016/0022-3115\(64\)90041-8](https://doi.org/10.1016/0022-3115(64)90041-8).
- [15] F.A. Nichols, Transport phenomena in nuclear fuels under severe temperature gradients, *J. Nucl. Mater.* 84 (1979) 1–25, [https://doi.org/10.1016/0022-3115\(79\)90147-8](https://doi.org/10.1016/0022-3115(79)90147-8).
- [16] D.R. O'Boyle, F.L. Brown, J.E. Sanecki, Solid fission product behavior in uranium-plutonium oxide fuel irradiated in a fast neutron flux, *J. Nucl. Mater.* 29 (1969) 27–42, [https://doi.org/10.1016/0022-3115\(69\)90124-X](https://doi.org/10.1016/0022-3115(69)90124-X).
- [17] M. Bober, C. Sari, G. Schumacher, Redistribution of plutonium and uranium in mixed (U, Pu) oxide fuel materials in a thermal gradient, *J. Nucl. Mater.* 39 (1971) 265–284.
- [18] M. Bober, C. Sari, G. Schumacher, Redistribution of uranium and plutonium during evaporation processes in mixed oxide fuels, *J. Nucl. Mater.* 40 (1971) 341–345.
- [19] M. Conte, M. Mouchino, F.K. Schmitz, Postirradiation observations of mixed oxides with initial addition of fission product elements, *Nucl. Technol.* 16 (1972) 143–155, <https://doi.org/10.13182/NT72-A31182>.
- [20] W.J. Lackey, F.J. Homan, A.R. Olsen, Porosity and actinide redistribution during irradiation of (U, Pu)O₂, *Nucl. Technol.* 16 (1972) 120–142, <https://doi.org/10.13182/NT72-A31181>.
- [21] J.K. Bahl, M.D. Freshley, Plutonium and fission product redistribution in mixed-oxide fuels during irradiation, *Nucl. Technol.* 15 (1972) 114–124, <https://doi.org/10.13182/NT72-A31142>.
- [22] M. Bober, G. Schumacher, D. Geithoff, Plutonium redistribution in fast reactor mixed oxide fuel pins, *J. Nucl. Mater.* 47 (1973) 187–197, https://acels-cdn.com/0022311573901013/1-s2.0-0022311573901013-main.pdf?_tid=45f58464-b051-11e7-8202-0000aab0f6c&acdnat=1507925057_d8a36b69a66cee677236524696ebf7ca. (Accessed 13 October 2017).
- [23] R.O. Meyer, Analysis of plutonium segregation and central-void formation in mixed-oxide fuels, *J. Nucl. Mater.* 50 (1974) 11–24, [https://doi.org/10.1016/0022-3115\(74\)90055-5](https://doi.org/10.1016/0022-3115(74)90055-5).
- [24] R.O. Meyer, C.R. Hann, D.D. Lanning, Effects of fissile atom segregation in light water reactor plutonium recycle fuels, *Nucl. Technol.* 27 (1975) 389–393.
- [25] M. Bober, H. Kleykamp, G. Schumacher, Investigation of radial plutonium redistribution in mixed oxide fuels irradiated in a fast flux, *Nucl. Technol.* 26 (1975) 172–182, <https://doi.org/10.13182/NT75-A24416>.
- [26] D. Haas, J. Van de Velde, M. Gaube, J. Ketels, C. Van Loon, Results of the postirradiation examinations of the Rapsodie-I experiment fuel pins, *Nucl. Technol.* 34 (1977) 75–88, <https://doi.org/10.13182/NT77-A31831>.
- [27] K. Tanaka, S. Miwa, I. Sato, T. Hirosawa, H. Obayashi, S.-I. Koyama, H. Yoshimochi, K. Tanaka, Microstructure and elemental distribution of americium-containing uranium plutonium mixed oxide fuel under a short-term irradiation test in a fast reactor, *J. Nucl. Mater.* 385 (2009) 407–412, <https://doi.org/10.1016/j.jnucmat.2008.12.028>.
- [28] K. Maeda, S. Sasaki, M. Kato, Y. Kihara, Radial redistribution of actinides in irradiated FR-MOX fuels, *J. Nucl. Mater.* 389 (2009) 78–84, <https://doi.org/10.1016/j.jnucmat.2009.01.010>.
- [29] K. Tanaka, S. Miwa, S.I. Sekine, H. Yoshimochi, H. Obayashi, S.I. Koyama, Restructuring and redistribution of actinides in Am-MOX fuel during the first 24 h of irradiation, *J. Nucl. Mater.* 440 (2013) 480–488, <https://doi.org/10.1016/j.jnucmat.2013.01.351>.
- [30] R.O. Meyer, D.R. O'Boyle, E.M. Butler, Effect of oxygen-to-metal ratio on plutonium redistribution in irradiated mixed-oxide fuels, *J. Nucl. Mater.* 47 (1973) 265–267.
- [31] H. Hoffmann, Crack formation, crack healing and porosity redistribution during irradiation of UO₂ and (U, Pu)O₂, *J. Nucl. Mater.* 54 (1974) 9–23, [https://doi.org/10.1016/0022-3115\(74\)90072-5](https://doi.org/10.1016/0022-3115(74)90072-5).
- [32] D.R. Olander, The kinetics of actinide redistribution by vapor migration in mixed oxide fuels (I). By cracks, *J. Nucl. Mater.* 49 (1973) 21–34, [https://doi.org/10.1016/0022-3115\(73\)90058-5](https://doi.org/10.1016/0022-3115(73)90058-5).
- [33] D. Olander, The conservation equations governing porosity and actinide redistribution in mixed-oxide fuels, *J. Nucl. Mater.* 47 (1973) 251–254.
- [34] S. Guarro, D.R. Olander, Actinide redistribution due to pore migration in hypostoichiometric mixed-oxide fuel pins, *J. Nucl. Mater.* 57 (1975) 136–144, [https://doi.org/10.1016/0022-3115\(75\)90253-6](https://doi.org/10.1016/0022-3115(75)90253-6).
- [35] C.F. Clement, M.W. Finnis, The movement of lenticular pores in mixed oxide (U, Pu)O₂ nuclear fuel elements, *J. Nucl. Mater.* 75 (1978) 115–124.
- [36] C.F. Clement, M.W. Finnis, Plutonium redistribution in mixed oxide (U,Pu)O₂ nuclear fuel elements, *J. Nucl. Mater.* 75 (1978) 193–200.
- [37] W. Breitung, H.U. Karow, K. Schretzmann, On the interpretation of vapor pressure measurements on oxide fuel at very-high temperatures for fast reactor safety analysis, *J. Nucl. Mater.* 60 (1975) 20–30.
- [38] T. Ishii, T. Asaga, An investigation of the Pu migration phenomena during irradiation in fast reactor, *J. Nucl. Mater.* 294 (2001) 13–17, [https://doi.org/10.1016/S0022-3115\(01\)00445-7](https://doi.org/10.1016/S0022-3115(01)00445-7).
- [39] Y. Ikusawa, K. Maed, M. Kato, M. Uno, Oxide-metal ratio dependence of central void formation of mixed oxide fuel irradiated in fast reactors, *Nucl. Technol.* 199 (2017) 83–95, <https://doi.org/10.1080/00295450.2017.1314748>.
- [40] C.T. Walker, M. Coquerelle, W. Goll, R. Manzel, Irradiation behaviour of MOX fuel: results of an EPMA investigation, *Nucl. Eng. Des.* 131 (1991) 1–16, [https://doi.org/10.1016/0029-5493\(91\)90313-7](https://doi.org/10.1016/0029-5493(91)90313-7).
- [41] W. Goll, H.-P. Fuchs, R. Manzel, F.U. Schlemmer, Irradiation behavior of UO₂/PuO₂ fuel in light water reactors, *Nucl. Technol.* 102 (1992) 29–46, <https://doi.org/10.13182/NT93-A34800>.
- [42] C.T. Walker, W. Goll, T. Matsumura, Effect of inhomogeneity on the level of fission gas and caesium release from OCOM MOX fuel during irradiation, *J. Nucl. Mater.* 228 (1996) 8–17.
- [43] C.T. Walker, W. Goll, T. Matsumura, Further observations on OCOM MOX fuel: microstructure in the vicinity of the pellet rim and fuel-cladding interaction, *J. Nucl. Mater.* 245 (1997) 169–178.
- [44] S.B. Fisher, R.J. White, P.M.A. Cook, S. Bremier, R.C. Corcoran, R. Stratton,

- C.T. Walker, P.K. Ivison, I.D. Palmer, Microstructure of irradiated SBR MOX fuel and its relationship to fission gas release, *J. Nucl. Mater.* 306 (2002) 153–172.
- [45] H. Kleykamp, Post-irradiation studies on LWR-MOX fuel fabricated by the optimized co-milling process, *J. Nucl. Mater.* 324 (2004) 198–202, <https://doi.org/10.1016/j.jnucmat.2003.10.004>.
- [46] L.J. Ott, R.N. Morris, Irradiation tests of mixed-oxide fuel prepared with weapons-derived plutonium, *J. Nucl. Mater.* 371 (2007) 314–328, <https://doi.org/10.1016/j.jnucmat.2007.05.030>.
- [47] J. Noirot, L. Desgranges, J. Lamontagne, Detailed characterisations of high burn-up structures in oxide fuels, *J. Nucl. Mater.* 372 (2008) 318–339, <https://doi.org/10.1016/j.jnucmat.2007.04.037>.
- [48] H.S. Kim, C.Y. Jong, B.H. Lee, J.Y. Oh, Y.H. Koo, Ceramography analysis of MOX fuel rods after an irradiation test, *Nucl. Eng. Technol.* 42 (2010) 576–581, <https://doi.org/10.5516/NET.2010.42.5.576>.
- [49] J.-Y. Colle, J.-P. Hiernaut, T. Wiss, O. Beneš, H. Thiele, D. Papaioannou, V.V. Rondinella, A. Sasahara, T. Sonoda, R.J.M. Konings, Fission product release and microstructure changes of irradiated MOX fuel at high temperatures, *J. Nucl. Mater.* 442 (2013) 330–340, <https://doi.org/10.1016/j.jnucmat.2013.09.022>.
- [50] R.L. Gibby, The effect of plutonium content on the thermal conductivity of (U, Pu)O₂ solid solutions, *J. Nucl. Mater.* 38 (1971) 163–177, [https://doi.org/10.1016/0022-3115\(71\)90040-7](https://doi.org/10.1016/0022-3115(71)90040-7).
- [51] T. Kameyama, Analyses plutonium by of burnup mixed neutron at oxide plutonium fuels and spots in light burnup in water reactors transport calculations, *J. Nucl. Sci. Technol.* 34 (1997) 551–558.
- [52] G. Sauer, W. Besenböck, Estimation of the influence of plutonium agglomerates in MOX fuel on the pellet temperature, in: Proc. 2007 International LWR Fuel Perform. Meet., 2007, pp. 347–356.
- [53] V.V. Rondinella, T. Wiss, The high burn-up structure in nuclear fuel, *Mater. Today* 13 (2010) 24–32, [https://doi.org/10.1016/S1369-7021\(10\)70221-2](https://doi.org/10.1016/S1369-7021(10)70221-2).
- [54] B. Lee, Y. Koo, H. Kim, J. Oh, Y. Tahk, D. Sohn, Recovery of thermal conductivity of MOX fuel with fission gas release, in: Proc. 2010 LWR Fuel Performance/TopFuel/WRFPM, 2010, pp. 689–697.
- [55] C. Jegou, M. Gennisson, S. Peugot, L. Desgranges, G. Guimbretière, M. Magnin, Z. Talip, P. Simon, Raman micro-spectroscopy of UOX and MOX spent nuclear fuel characterization and oxidation resistance of the high burn-up structure, *J. Nucl. Mater.* 458 (2015) 343–349, <https://doi.org/10.1016/j.jnucmat.2014.12.072>.
- [56] C.T. Walker, Electron probe microanalysis of irradiated nuclear fuel: an overview, *J. Anal. At. Spectrom.* 14 (1999) 447–454, <https://doi.org/10.1039/a086761i>.
- [57] H. Bernard, Advanced fuel fabrication, *J. Nucl. Mater.* 166 (1989) 105–111.
- [58] R. Güldner, H. Schmidt, Optimization of process parameters for the sintering of MOX fuel, *J. Nucl. Mater.* 178 (1991) 152–157, [https://doi.org/10.1016/0022-3115\(91\)90380-P](https://doi.org/10.1016/0022-3115(91)90380-P).
- [59] D. Haas, A. Vandergheynst, J. van Vliet, R. Lorenzelli, J.-L. Nigon, Mixed-oxide fuel fabrication technology and experience at the belgonucléaire and CFCa plants and further developments for the MELOX plant, *Nucl. Technol.* 106 (1994) 60–82, <https://doi.org/10.13182/NT94-A34950>.
- [60] D.E. Burkes, R.S. Fielding, D.L. Porter, M.K. Meyer, B.J. Makenas, A US perspective on fast reactor fuel fabrication technology and experience. Part II: ceramic fuels, *J. Nucl. Mater.* 393 (2009) 1–11, <https://doi.org/10.1016/j.jnucmat.2009.04.023>.
- [61] R. Vauchy, A.-C. Robisson, F. Audubert, F. Hodaj, Ceramic processing of uranium–plutonium mixed oxide fuels (U₁–yPu)₂O₅ with high plutonium content, *Ceram. Int.* 40 (2014) 10991–10999, <https://doi.org/10.1016/j.ceramint.2014.03.104>.
- [62] H. Bernard, Advanced fuel fabrication, *J. Nucl. Mater.* 166 (1989) 105–111, [https://doi.org/10.1016/0022-3115\(89\)90182-7](https://doi.org/10.1016/0022-3115(89)90182-7).
- [63] M.D. Freshley, UO₂–PuO₂ – a demonstrated fuel for plutonium utilization in thermal reactors, *Nucl. Technol.* 18 (1973) 141–170, <https://doi.org/10.13182/NT73-A31284>.
- [64] A. Renard, N. Mostin, Safety aspects of micro-heterogeneities in LWR mixed oxide fuels, *J. Nucl. Mater.* 81 (1979) 31–38.
- [65] G. Oudinet, I. Muñoz-Villard, L. Aufore, M.-J. Gotta, J.M. Becker, G. Chiarelli, R. Castelli, Characterization of plutonium distribution in MIMAS MOX by image analysis, *J. Nucl. Mater.* 375 (2008) 86–94, <https://doi.org/10.1016/j.jnucmat.2007.10.013>.
- [66] K.V. Vrinda Devi, T. Soreng, J.P. Panakkal, H.S. Kamath, Nondestructive determination of relative plutonium content in MOX fuel pins for pressurized heavy water reactors using passive gamma scanning, *Nucl. Technol.* 164 (2008) 305–308, <https://doi.org/10.13182/NT08-A4028>.
- [67] K.V. Vrinda Devi, J.P. Panakkal, Quantification of plutonium heterogeneity in (U, Pu) mixed oxide fuel using Passive Gamma Scanning, *Nucl. Eng. Des.* 255 (2013) 132–137, <https://doi.org/10.1016/j.nucengdes.2012.10.018>.
- [68] S. Kodaira, M. Kurano, T. Hosogane, F. Ishikawa, T. Kageyama, M. Sato, M. Kayano, N. Yasuda, S. Kodaira, M. Kurano, T. Hosogane, F. Ishikawa, T. Kageyama, M. Sato, Note : application of CR-39 plastic nuclear track detectors for quality assurance of mixed oxide fuel pellets, *Rev. Sci. Instrum.* 86 (2015) 3–6, <https://doi.org/10.1063/1.4919904>.
- [69] C. Baghra, D.B. Sathe, J. Sharma, N. Walinjkar, P.G. Behere, M. Afzal, A. Kumar, Evaluation of micro-homogeneity in plutonium based nuclear reactor fuel pellets by alpha-autoradiography technique, *J. Nucl. Mater.* 467 (2015) 730–741, <https://doi.org/10.1016/j.jnucmat.2015.10.058>.
- [70] D. Staicu, M. Barker, Thermal conductivity of heterogeneous LWR MOX fuels, *J. Nucl. Mater.* 442 (2013) 46–52, <https://doi.org/10.1016/j.jnucmat.2013.08.024>.
- [71] M. Amaya, J. Nakamura, F. Nagase, T. Fuketa, Thermal conductivity evaluation of high burnup mixed-oxide (MOX) fuel pellet, *J. Nucl. Mater.* 414 (2011) 303–308, <https://doi.org/10.1016/j.jnucmat.2011.04.020>.
- [72] D. Staicu, C. Cozzo, G. Pagliosa, D. Papaioannou, S. Bremier, V.V. Rondinella, C.T. Walker, A. Sasahara, Thermal conductivity of homogeneous and heterogeneous MOX fuel with up to 44MWd/kgHM burn-up, *J. Nucl. Mater.* 412 (2011) 129–137, <https://doi.org/10.1016/j.jnucmat.2011.02.042>.
- [73] M.D. Freshley, E.A. Aitken, D.C. Wadekamper, R.L. Johnson, W.G. Lussie, Behavior of discrete plutonium-dioxide particles in mixed-oxide fuel during rapid power transients, *Nucl. Technol.* 15 (1972) 239–248, <https://doi.org/10.13182/NT72-A31148>.
- [74] H. Kleykamp, The chemical state of the fission products in oxide fuels, *J. Nucl. Mater.* 131 (1985) 221–246.
- [75] J.I. Brammall, R.M. Sharpe, D. Thom, G. Yates Ukaea, Metallic fission-product inclusions in irradiated oxide fuels, *J. Nucl. Mater.* (1968) 201–215.
- [76] D.R. O'Boyle, F.L. Brown, A.E. Dwight, Analysis of fission product ingots formed in uranium-plutonium oxide irradiated in EBR-II, *J. Nucl. Mater.* 35 (1970) 257–266.
- [77] H. Kleykamp, J.O. Paschoal, R. Pejsa, F. Thümmler, Composition and structure of fission product precipitates in irradiated oxide fuels: correlation with phase studies in the Mo-Ru-Rh-Pd and BaO-UO₂-ZrO₂-MoO₂ Systems, *J. Nucl. Mater.* 130 (1985) 426–433, [https://doi.org/10.1016/0022-3115\(85\)90329-0](https://doi.org/10.1016/0022-3115(85)90329-0).
- [78] A.E. Dwight, D.R. O'Boyle, Phase studies on fission product alloys, *J. Nucl. Mater.* 136 (1985) 280–283, [https://doi.org/10.1016/0022-3115\(85\)90015-7](https://doi.org/10.1016/0022-3115(85)90015-7).
- [79] H. Kleykamp, The chemical state of fission products in oxide fuels at different stages of the nuclear fuel cycle, *Nucl. Technol.* 80 (1988) 412–422, <https://doi.org/10.13182/NT88-A34065>.
- [80] S. Yamanaka, K. Kurosaki, Thermophysical properties of Mo–Ru–Rh–Pd alloys, *J. Alloy. Comp.* 353 (2003) 269–273, [https://doi.org/10.1016/S0925-8388\(02\)01211-2](https://doi.org/10.1016/S0925-8388(02)01211-2).
- [81] D. Cui, V.V. Rondinella, J.A. Fortner, A.J. Kropf, L. Eriksson, D.J. Wronkiewicz, K. Spahiu, Characterization of alloy particles extracted from spent nuclear fuel, *J. Nucl. Mater.* 420 (2012) 328–333, <https://doi.org/10.1016/j.jnucmat.2011.10.015>.
- [82] M. Teague, B. Gorman, B. Miller, J. King, EBSD and TEM characterization of high burn-up mixed oxide fuel, *J. Nucl. Mater.* 444 (2014) 475–480, <https://doi.org/10.1016/j.jnucmat.2013.10.037>.
- [83] G. Giacchetti, C. Sari, Behavior of molybdenum in mixed-oxide fuel, *Nucl. Technol.* 31 (1976) 62–69, <https://doi.org/10.13182/NT76-A31699>.
- [84] F. D'Annucci, C. Sari, G. Schumacher, Migration of metallic fission products in reactor oxide fuels, *Nucl. Technol.* 35 (1977) 80–86, <https://doi.org/10.13182/NT77-A31851>.
- [85] L.A. Lawrence, J.A. Christensen, Molybdenum distribution in irradiated oxide fuels, *J. Nucl. Mater.* 37 (1970) 248–250.
- [86] F.T. Ewart, R.G. Taylor, J.M. Horspool, G. James, The chemical effects of composition changes in irradiated oxide fuel materials II - fission product segregation and chemical equilibria, *J. Nucl. Mater.* 61 (1976) 254–270.
- [87] M. Tourasse, M. Boidron, B. Pasquet, Fission product behaviour in Phenix fuel pins at high burnup, *J. Nucl. Mater.* 188 (1992) 49–57.
- [88] I. Sato, Behavior of metallic fission products in uranium- plutonium mixed oxide fuel, *J. Nucl. Mater.* 273 (1999) 239–247.
- [89] K. Maeda, T. Asaga, Change of fuel-to-cladding gap width with the burn-up in FBR MOX fuel irradiated to high burn-up, *J. Nucl. Mater.* (2004) 1–10, <https://doi.org/10.1016/j.jnucmat.2004.01.003>.
- [90] K. Maeda, K. Tanaka, T. Asaga, H. Furuya, Distributions of volatile fission products in or near the fuel-cladding gap of the FBR MOX fuel pins irradiated to high burn-up, *J. Nucl. Mater.* 344 (2005) 274–280, <https://doi.org/10.1016/j.jnucmat.2005.04.054>.
- [91] H. Kleykamp, J.O. Paschoal, R. Pejsa, F. Thümmler, Composition and structure of fission product precipitates in irradiated oxide fuels: correlation with phase studies in the Mo-Ru-Rh-Pd and BaO-UO₂-ZrO₂-MoO₂ Systems, *J. Nucl. Mater.* 130 (1985) 426–433, [https://doi.org/10.1016/0022-3115\(85\)90329-0](https://doi.org/10.1016/0022-3115(85)90329-0).
- [92] J.H. Davies, F.T. Ewart, The chemical effects of composition changes in irradiated oxide fuel materials, *J. Nucl. Mater.* 41 (1971) 143–155, [https://doi.org/10.1016/0022-3115\(71\)90074-2](https://doi.org/10.1016/0022-3115(71)90074-2).
- [93] H. Matzke, J. Ottaviani, D. Pellettiero, J. Rouault, Oxygen potential of high burn-up fast breeder oxide fuel, *J. Nucl. Mater.* 160 (1988) 142–146.
- [94] M. Kato, T. Tamura, K. Konashi, Oxygen potentials of mixed oxide fuels for fast reactors, *J. Nucl. Mater.* 385 (2009) 419–423, <https://doi.org/10.1016/j.jnucmat.2008.12.012>.
- [95] H. Kleykamp, The solubility of selected fission products in UO₂ and (U, Pu)O₂, *J. Nucl. Mater.* 206 (1993) 82–86, [https://doi.org/10.1016/0022-3115\(93\)90236-R](https://doi.org/10.1016/0022-3115(93)90236-R).
- [96] C. Sari, Solubility and migration of fission product barium in oxide fuel, *J. Nucl. Mater.* 79 (1979) 255–259.
- [97] I. Sato, H. Furuya, T. Arima, K. Idemitsu, K. Yamamoto, Behavior of fission products zirconium and barium in fastreactor fuel irradiated to high burnup, *J. Nucl. Sci. Technol.* 36 (1999) 775–780, <https://doi.org/10.1080/18811248.1999.9726267>.

- [98] T. Matsuda, S. Yamanaka, K. Kurosaki, M. Uno, S.-I. Kobayashi, Heat capacity measurement of BaU₃, *J. Alloy. Comp.* 322 (2001) 77–81, [https://doi.org/10.1016/S0925-8388\(01\)01263-4](https://doi.org/10.1016/S0925-8388(01)01263-4).
- [99] S. Yamanaka, K. Kurosaki, T. Matsuda, Thermophysical properties of BaUO₃, *J. Nucl. Mater.* 294 (2001) 99–103, <http://www.sciencedirect.com/science/article/pii/S0022311501004743%5Cnpapers2://publication/uuid/DC566C65-F555-4C9D-8740-F710EB24C1E8>.
- [100] S. Yamanaka, K. Kurosaki, T. Matsuda, S.I. Kobayashi, Thermal properties of SrCeO₃, *J. Alloy. Comp.* 352 (2003) 52–56, [https://doi.org/10.1016/S0925-8388\(02\)01133-7](https://doi.org/10.1016/S0925-8388(02)01133-7).
- [101] S. Yamanaka, M. Fujikane, T. Hamaguchi, H. Muta, T. Oyama, T. Matsuda, S.I. Kobayashi, K. Kurosaki, Thermophysical properties of BaZrO₃ and BaCeO₃, *J. Alloy. Comp.* 359 (2003) 109–113, [https://doi.org/10.1016/S0925-8388\(03\)00214-7](https://doi.org/10.1016/S0925-8388(03)00214-7).
- [102] S. Yamanaka, T. Hamaguchi, T. Oyama, T. Matsuda, S. Kobayashi, K. Kurosaki, Heat capacities and thermal conductivities of perovskite type BaZrO₃ and BaCeO₃, *J. Alloy. Comp.* 359 (2003) 1–4, [https://doi.org/10.1016/S0925-8388\(03\)00137-3](https://doi.org/10.1016/S0925-8388(03)00137-3).
- [103] S. Yamanaka, T. Maekawa, H. Muta, T. Matsuda, S.I. Kobayashi, K. Kurosaki, Thermophysical properties of SrHfO₃ and SrRuO₃, *J. Solid State Chem.* 177 (2004) 3484–3489, <https://doi.org/10.1016/j.jssc.2004.05.039>.
- [104] S. Yamanaka, K. Kurosaki, T. Maekawa, T. Matsuda, S.I. Kobayashi, M. Uno, Thermochemical and thermophysical properties of alkaline-earth perovskites, *J. Nucl. Mater.* 344 (2005) 61–66, <https://doi.org/10.1016/j.jnucmat.2005.04.017>.
- [105] K. Tanaka, I. Sato, T. Hirosawa, K. Kurosaki, H. Muta, S. Yamanaka, Thermal conductivity of BaPuO₃ at temperatures from 300 to 1500 K, *J. Nucl. Mater.* 414 (2011) 316–319, <https://doi.org/10.1016/j.jnucmat.2011.04.057>.
- [106] T. Hirosawa, I. Sato, Burnup dependence of melting temperature of FBR mixed oxide fuels irradiated to high burnup, *J. Nucl. Mater.* 418 (2011) 207–214, <https://doi.org/10.1016/j.jnucmat.2011.07.001>.
- [107] M.G. Adamson, E.A. Aitken, R.W. Caputi, Experimental and thermodynamic evaluation of the melting behavior of irradiated oxide fuels, *J. Nucl. Mater.* 130 (1985) 349–365, [https://doi.org/10.1016/0022-3115\(85\)90323-X](https://doi.org/10.1016/0022-3115(85)90323-X).
- [108] M.G. Adamson, E.A. Aitken, O. Ridge, O. Ridge, Chemical thermodynamics of Cs and Te fission product interactions in irradiated LMFBR mixed-oxide fuel pins, *J. Nucl. Mater.* 130 (1985) 375–392.
- [109] T. Uwaba, M. Ito, K. Maeda, Diametral strain of fast reactor MOX fuel pins with austenitic stainless steel cladding irradiated to high burnup, *J. Nucl. Mater.* 416 (2011) 350–357, <https://doi.org/10.1016/j.jnucmat.2011.06.033>.
- [110] H. Furuya, S. Ukai, S. Shikakura, Y. Tsuchiichi, K. Idemitsu, Axial distribution of cesium in heterogeneous FBR fuel pins, *J. Nucl. Mater.* 201 (1993) 46–53, [https://doi.org/10.1016/0022-3115\(93\)90158-U](https://doi.org/10.1016/0022-3115(93)90158-U).
- [111] K. Kurosaki, K. Tanaka, M. Osaka, Y. Ohishi, Chemical states of fission products and actinides in irradiated oxide fuels analyzed by thermodynamic calculation and post-irradiation examination, *Prog. Nucl. Sci. Technol.* 2 (2011) 5–8, <https://doi.org/10.15669/pnst.2.5>.
- [112] M. Inoue, K. Maeda, K. Katsuyama, K. Tanaka, K. Mondo, M. Hisada, Fuel-to-cladding gap evolution and its impact on thermal performance of high burnup fast reactor type uranium-plutonium oxide fuel pins, *J. Nucl. Mater.* 326 (2004) 59–73, <https://doi.org/10.1016/j.jnucmat.2003.12.015>.
- [113] T. Ishii, T. Mizuno, Thermal conductivity of cesium molybdate Cs₂MoO₄, *J. Nucl. Mater.* 231 (1996) 242–244, [https://doi.org/10.1016/0022-3115\(96\)00390-X](https://doi.org/10.1016/0022-3115(96)00390-X).
- [114] T. Ishii, T. Mizuno, An investigation of the thermal conductivity of Cs₂MoO₄, *J. Nucl. Mater.* 247 (1997) 82–85.
- [115] K. Minato, M. Takano, K. Fukuda, S. Sato, H. Ohashi, Thermal expansion and thermal conductivity of cesium molybdate, *J. Alloy. Comp.* 255 (1997) 18–23, [https://doi.org/10.1016/S0925-8388\(96\)02841-1](https://doi.org/10.1016/S0925-8388(96)02841-1).
- [116] G. Wallez, P.E. Raison, A.L. Smith, N. Clavier, N. Dacheux, High-temperature behavior of dicesium molybdate Cs₂MoO₄: implications for fast neutron reactors, *J. Solid State Chem.* 215 (2014) 225–230, <https://doi.org/10.1016/j.jssc.2014.04.003>.
- [117] M. Takano, K. Minato, K. Fukuda, S. Sato, H. Ohashi, Thermal expansion and thermal conductivity of cesium uranates, *J. Nucl. Sci. Technol.* 35 (1998) 485–493.
- [118] J.C. Melis, J.P. Piron, L. Roche, Fuel modeling at high burn-up: recent development of the GERMINAL code, *J. Nucl. Mater.* 204 (1993) 188–193, [https://doi.org/10.1016/0022-3115\(93\)90216-L](https://doi.org/10.1016/0022-3115(93)90216-L).
- [119] J.-C. Melis, H. Plitz, R. Thetford, Highly irradiated CABRI fuel behaviour up to melting : JOG tests in CABRI, *J. Nucl. Mater.* 204 (1993) 212–216.
- [120] M.A. Mignanielli, R. Thetford, Chemical modelling in the TRAFIC code, *J. Nucl. Mater.* 204 (1993) 173–179, [https://doi.org/10.1016/0022-3115\(93\)90214-J](https://doi.org/10.1016/0022-3115(93)90214-J).
- [121] T. Ozawa, T. Abe, Development and verifications of fast reactor fuel design code CEPTAR, *Nucl. Technol.* 156 (2006) 39–55, <https://doi.org/10.13182/NT156-39>.
- [122] T. Uwaba, T. Mizuno, J. Nemoto, I. Ishitani, M. Ito, Development of a mixed oxide fuel pin performance analysis code "cEDAR": models and analyses of fuel pin irradiation behavior, *Nucl. Eng. Des.* 280 (2014) 27–36, <https://doi.org/10.1016/j.nucengdes.2014.08.032>.
- [123] K. Maeda, T. Asaga, Change of fuel-to-cladding gap width with the burn-up in FBR MOX fuel irradiated to high burn-up, *J. Nucl. Mater.* 327 (2004) 1–10, <https://doi.org/10.1016/j.jnucmat.2004.01.003>.
- [124] K. Maeda, Ceramic fuel – cladding interaction, in: first ed., in: R.J.M. Konings (Ed.), *Compr. Nucl. Mater.*, vol. 3, Elsevier Ltd, Waltham, MA, 2012, pp. 443–483, <https://doi.org/10.1016/B978-0-08-056033-5.09009-1>.
- [125] L.A. Lawrence, Fuel/cladding chemical interaction in mixed-oxide fuel at high burnup, *Nucl. Technol.* 64 (1984) 139–153, <https://doi.org/10.13182/NT84-A3337>.
- [126] D.C. Fee, C.E. Johnson, Fuel-cladding chemical interaction in uranium-plutonium oxide fast reactor fuel pins, *J. Nucl. Mater.* 96 (1981) 80–104, [https://doi.org/10.1016/0022-3115\(81\)90221-X](https://doi.org/10.1016/0022-3115(81)90221-X).
- [127] L.A. Neimark, J.D.B. Lambert, W.F. Murphy, C.W. Renfro, Performance of mixed-oxide fuel elements to 11 at.% burnup, *Nucl. Technol.* 16 (1972) 75–88, <https://doi.org/10.13182/NT72-A3117>.
- [128] O. Götzmann, P. Hofmann, F. Thümmler, Attack upon the cladding of oxide fuel pins by fuel and fission products, *J. Nucl. Mater.* 52 (1974) 33–50, [https://doi.org/10.1016/0022-3115\(74\)90023-3](https://doi.org/10.1016/0022-3115(74)90023-3).
- [129] M.G. Adamson, On the Cs, Te fission product induced attack and embrittlement of stainless steel cladding in oxide fuel pins, *J. Nucl. Mater.* 132 (1985) 160–166.
- [130] O. Götzmann, A thermodynamic model for the attack behaviour in stainless steel clad oxide fuel pins, *J. Nucl. Mater.* 84 (1979) 39–54, [https://doi.org/10.1016/0022-3115\(79\)90149-1](https://doi.org/10.1016/0022-3115(79)90149-1).
- [131] K. Konashi, K. Kamimura, Y. Yokouchi, Model for fuel/cladding chemical interaction, *Nucl. Technol.* 72 (1986) 328–337, <https://doi.org/10.13182/NT86-A3371>.
- [132] R. Viswanathan, Fuel clad chemical interactions in fast reactor MOX fuels, *J. Nucl. Mater.* 444 (2014) 101–111, <https://doi.org/10.1016/j.jnucmat.2013.09.044>.
- [133] L.A. Lawrence, D.C. Hata, J.W. Weber, The effects of stoichiometry on cladding attack in UO₂-PuO₂, *Nucl. Technol.* 42 (1979) 195–206, <https://doi.org/10.13182/NT79-A32150>.
- [134] M.H. Bradbury, S. Pickering, W.H. Whitlow, A proposed mechanism for internal cladding corrosion in LMFBR mixed oxide fuel pins, *J. Nucl. Mater.* 78 (1978) 272–280, [https://doi.org/10.1016/0022-3115\(78\)90448-8](https://doi.org/10.1016/0022-3115(78)90448-8).
- [135] M. Kato, K. Morimoto, H. Sugata, K. Konashi, M. Kashimura, T. Abe, Solidus and liquidus temperatures in the UO₂ – PuO₂ system, *J. Nucl. Mater.* 373 (2008) 237–245, <https://doi.org/10.1016/j.jnucmat.2007.06.002>.
- [136] M. Kato, K. Morimoto, H. Sugata, K. Konashi, M. Kashimura, T. Abe, Solidus and liquidus of plutonium and uranium mixed oxide, *J. Alloy. Comp.* 452 (2008) 48–53, <https://doi.org/10.1016/j.jallcom.2007.01.183>.
- [137] J. Nakamura, M. Amaya, F. Nagase, T. Fuketa, Thermal conductivity change in high burnup MOX fuel pellet, *J. Nucl. Sci. Technol.* 46 (2009) 944–952, <https://doi.org/10.1080/18811248.2009.9711603>.
- [138] N. Nakae, H. Akiyama, H. Miura, T. Baba, K. Kamimura, S. Kurematsu, Y. Kosaka, A. Yoshino, T. Kitagawa, Thermal property change of MOX and UO₂ irradiated up to high burnup of 74 GWd/t, *J. Nucl. Mater.* 440 (2013) 515–523, <https://doi.org/10.1016/j.jnucmat.2013.02.057>.
- [139] K. Morimoto, M. Kato, M. Ogasawara, Thermal diffusivity measurement of (U, Pu)O₂-x at high temperatures up to 2190 K, *J. Nucl. Mater.* 443 (2013) 286–290, <https://doi.org/10.1016/j.jnucmat.2013.07.048>.
- [140] T. Matsumoto, T. Arima, Y. Inagaki, K. Idemitsu, M. Kato, T. Uchida, Investigation of O/M ratio effect on thermal conductivity of oxide nuclear fuels by non-equilibrium molecular dynamics calculation, *J. Nucl. Mater.* 440 (2013) 580–585, <https://doi.org/10.1016/j.jnucmat.2013.04.019>.
- [141] M. Kato, K. Morimoto, T. Tamura, T. Sunaoshi, K. Konashi, S. Aono, M. Kashimura, Oxygen chemical diffusion in hypo-stoichiometric MOX, *J. Nucl. Mater.* 389 (2009) 416–419, <https://doi.org/10.1016/j.jnucmat.2009.02.018>.
- [142] R. Vauchy, R.C. Belin, A.-C. Robisson, F. Hodaj, Effect of cooling rate on achieving thermodynamic equilibrium in uranium-plutonium mixed oxides, *J. Nucl. Mater.* 469 (2016) 125–132, <https://doi.org/10.1016/j.jnucmat.2015.11.049>.
- [143] M. Kato, K. Konashi, N. Nakae, Analysis of oxygen potential of (U 0.7 Pu 0.3)O_{2-x} and (U 0.8 Pu 0.2)O_{2-x} based on point defect chemistry, *J. Nucl. Mater.* 389 (2009) 164–169, <https://doi.org/10.1016/j.jnucmat.2009.01.023>.
- [144] M. Kato, Y. Ikusawa, T. Sunaoshi, A.T. Nelson, K.J. McClellan, Thermal expansion measurement of (U,Pu)O_{2-x} in oxygen partial pressure-controlled atmosphere, *J. Nucl. Mater.* 469 (2016) 223–227, <https://doi.org/10.1016/j.jnucmat.2015.11.048>.
- [145] R. Böhler, M.J. Welland, D. Prieur, P. Cakir, T. Vitova, T. Pruessmann, I. Pidchenko, C. Hennig, C. Guéneau, R.J.M. Konings, D. Manara, Recent advances in the study of the UO₂–PuO₂ phase diagram at high temperatures, *J. Nucl. Mater.* 448 (2014) 330–339, <https://doi.org/10.1016/j.jnucmat.2014.02.029>.
- [146] F. De Bruycker, K. Boboridis, R.J.M. Konings, M. Rini, R. Eloirdi, C. Guéneau, N. Dupin, D. Manara, On the melting behaviour of uranium/plutonium mixed dioxides with high-Pu content: a laser heating study, *J. Nucl. Mater.* 419 (2011) 186–193, <https://doi.org/10.1016/j.jnucmat.2011.08.028>.
- [147] M. Kato, T. Tamura, K. Konashi, Oxygen potentials of mixed oxide fuels for fast reactors, *J. Nucl. Mater.* 385 (2009) 419–423, <https://doi.org/10.1016/j.jnucmat.2008.12.012>.
- [148] J. Washington, J. King, Z. Shayer, Target fuels for plutonium and minor actinide transmutation in pressurized water reactors, *Nucl. Eng. Des.* 313 (2017) 53–72, <https://doi.org/10.1016/j.nucengdes.2016.11.033>.
- [149] E. Martinez, J. Ramón Ramírez, G. Alonso, Actinides recycling assessment in a thermal reactor, *Ann. Nucl. Energy* 79 (2015) 51–60, <https://doi.org/10.1016/j.anucene.2015.01.014>.
- [150] K. Morimoto, M. Kato, M. Ogasawara, M. Kashimura, Thermal conductivity of

- (U,Pu,Np)O₂ solid solutions, *J. Nucl. Mater.* 389 (2009) 179–185, <https://doi.org/10.1016/j.jnucmat.2009.01.026>.
- [151] K. Morimoto, M. Kato, M. Ogasawara, M. Kashimura, T. Abe, Thermal conductivities of (U, Pu, Am)O₂ solid solutions, *J. Alloy. Comp.* 452 (2008) 54–60, <https://doi.org/10.1016/j.jallcom.2006.12.159>.
- [152] K. Maeda, S. Sasaki, M. Kato, Y. Kihara, Short-term irradiation behavior of minor actinide doped uranium plutonium mixed oxide fuels irradiated in an experimental fast reactor, *J. Nucl. Mater.* 385 (2009) 413–418, <https://doi.org/10.1016/j.jnucmat.2008.12.041>.
- [153] A. Rico, M.A. Martin-Rengel, J. Ruiz-Hervias, J. Rodriguez, F.J. Gomez-Sanchez, Nanoindentation measurements of the mechanical properties of zirconium matrix and hydrides in unirradiated pre-hydrided nuclear fuel cladding, *J. Nucl. Mater.* 452 (2014) 69–76, <https://doi.org/10.1016/J.JNUCMAT.2014.04.045>.
- [154] A. Reichardt, A. Lupinacci, D. Frazer, N. Bailey, H. Vo, C. Howard, Z. Jiao, A.M. Minor, P. Chou, P. Hosemann, Nanoindentation and *in situ* micro-compression in different dose regimes of proton beam irradiated 304 SS, *J. Nucl. Mater.* 486 (2017) 323–331, <https://doi.org/10.1016/J.JNUCMAT.2017.01.036>.
- [155] D. Frazer, J. Szornel, D.L. Krumwiede, K.A. Terrani, P. Hosemann, Evaluation of the mechanical properties of TRISO particles using nanoindentation and ring compression testing, *Exp. Mech.* 57 (2017) 1081–1090, <https://doi.org/10.1007/s11340-017-0277-z>.
- [156] D.H. Hurley, R.S. Schley, M. Khafizov, B.L. Wendt, Local measurement of thermal conductivity and diffusivity, *Rev. Sci. Instrum.* 86 (2015) 1–8, <https://doi.org/10.1063/1.4936213>.
- [157] L.F. He, B. Valderrama, A.-R. Hassan, J. Yu, M. Gupta, J. Pakarinen, H.B. Henderson, J. Gan, M.A. Kirk, A.T. Nelson, M.V. Manuel, A. El-Azab, T.R. Allen, Bubble formation and Kr distribution in Kr-irradiated UO₂, *J. Nucl. Mater.* 456 (2015) 125–132, <https://doi.org/10.1016/J.JNUCMAT.2014.09.026>.
- [158] L. Desgranges, C. Valot, B. Pasquet, Characterisation of irradiated nuclear fuel with SIMS, *Appl. Surf. Sci.* 252 (2006) 7048–7050, <https://doi.org/10.1016/J.APSUSC.2006.02.256>.
- [159] M. Teague, B. Gorman, Utilization of dual-column focused ion beam and scanning electron microscope for three dimensional characterization of high burn-up mixed oxide fuel, *Prog. Nucl. Energy* 72 (2014) 67–71, <https://doi.org/10.1016/j.pnucene.2013.08.006>.
- [160] M.C. Teague, B.S. Fromm, M.R. Tonks, D.P. Field, Using coupled mesoscale experiments and simulations to investigate high burn-up oxide fuel thermal conductivity, *JOM-J. Miner. Met. Mater. Soc.* 66 (2014) 2569–2577, <https://doi.org/10.1007/s11837-014-1160-3>.
- [161] M. Teague, M. Tonks, S. Novascone, S. Hayes, Microstructural modeling of thermal conductivity of high burn-up mixed oxide fuel, *J. Nucl. Mater.* 444 (2014) 161–169, <https://doi.org/10.1016/j.jnucmat.2013.09.035>.
- [162] H. Kleykamp, The chemical state of the fission products in oxide fuels, *J. Nucl. Mater.* 131 (1985) 221–246, [https://doi.org/10.1016/0022-3115\(85\)90460-X](https://doi.org/10.1016/0022-3115(85)90460-X).